UNIVERSITA' DEGLI STUDI DI PADOVA

Sede Amministrativa: Università degli Studi di Padova

Dipartimento di Innovazione Meccanica e Gestionale

SCUOLA DI DOTTORATO DI RICERCA IN INGEGNERIA INDUSTRIALE
INDIRIZZO: INGEGNERIA DELLA PRODUZIONE INDUSTRIALE
CICLO XXI

MODELLING OF THE MANNESMANN EFFECT IN TUBE PIERCING

Direttore della Scuola: Ch.mo Prof. Paolo F. Bariani
Supervisore: Ch.mo Prof. Paolo F. Bariani

Dottorando: Silvio Fanini

True knowledge exists in knowing that you know nothing.

Socrates

TABLE OF CONTENTS

ACKNOWLEDGMENTS

This work was coordinated by Prof. Paolo Bariani to whom I express my sincerest gratitude.
I am thankful to Prof. Yvan Chastel, to his staff and to the Mecanum group for my unforgettable time in CEMEF.
A particular thanks to Stefania and Andrea for their endless help, the trust they placed in me and most of all their solid friendship.
I would also like to thank my colleagues at DIMEG for their invaluable support during these years.
My gratitude goes to my family, for their wonderful support over the years. This goal could not have been reached without them.

Silvio Fanini

Padova, December 2008

CONFIDENTIALITY NOTE

This work has been developed thanks to a research project in collaboration with one of the main world seamless tube manufacturer.
For this reason, some information are confidential and they have been hidden in this public copy of the thesis.

ABSTRACT

Seamless tube manufacturing utilises continuous cast cylindrical billets that, after piercing, are rolled until a specified diameter, thickness and length are reached. The hollow part can be industrially obtained through cross roll piercing. The main characteristic of this process is the local failure at the billet centre due to the so-called Mannesmann Effect. In general the cylindrical billet is introduced into the piecing mill after a pre-heating stage, it is dragged and radially deformed by two skew conical rolls that create the stress state generating the internal cavity and then it is effectively pierced by a plug that enlarges the axial crack. The knowledge of the industrial parameters, which determine the beginning and the propagation of the axial fracture, is crucial because it determines the optimal position of the plug in order to grant the best quality of the tube and service life of the plug.

Despite the vast industrial experience, the scientific knowledge of the Mannesmann Effect is quite limited. Fracture initiation has been widely studied at room temperature and many contributions can be found in scientific literature, but there is a substantial lack in fracture modelling when applied to forming operations at elevated temperatures.

The objective of this work is to develop a reliable numerical model capable to describe the industrial conditions that lead to Mannesmann fracture through the implementation into a commercial FE code of a damage law appropriately calibrated on experimental material behaviour.

experimentally it can be noted that the solidification phase of steel after the continuous casting process provokes a differentiation of the billet material in terms of the amount of voids fraction and phase distribution that is reflected on its behaviour during the forming operation. Material workability under process conditions is investigated through hot tensile tests carried out on specimens machined from a continuous cast billet and microscopic observations are performed in order to correlate the sample location in the billet section with its micro-structural characteristics.

The fracture condition characterization is possible using a damage model according to the Lemaitre formulation and the identification of damage parameters is based on the inverse analysis on hot tensile test results. In particular, a modification to the standard damage law is adopted in order to

describe the different behaviour of the material in the billet section and to take into account the effect of porosity and phase distribution on the initial material state.

Finally, the developed numerical model is validated, through the comparison between numerical results and industrial trials of non-plug piercing, showing that there is a good agreement in regards to the length and initiation site of the Mannesmann cone fracture.

SOMMARIO

La produzione di tubi in acciaio senza saldatura si basa sull'utilizzo di barre cilindriche ottenute per colata continua che, dopo aver subito il processo di perforazione, vengono sottoposte a diverse operazioni di laminazione per l'ottenimento delle caratteristiche specificate in termini di lunghezza e spessore del tubo finale. Industrialmente il forato è ottenuto mediante il processo di perforazione obliqua, la cui caratteristica principale è una frattura lungo l'asse longitudinale della billetta che si crea per il cosiddetto Effetto Mannesmann.
Nel processo industriale, in seguito a una fase di riscaldamento, la billetta cilindrica viene introdotta nell'impianto di perforazione, trascinata e deformata dall'azione di due rulli tronco-conici ad assi sghembi che generano lo stato di sollecitazione caratteristico per la comparsa della frattura interna. Solo a questo punto la billetta viene effettivamente perforata da un mandrino che svolge la funzione di allargare la cavità ottenuta longitudinalmente e laminare le pareti interne del forato.
La conoscenza delle condizioni industriali di laminazione che determinano la comparsa e della frattura lungo l'asse della billetta e la sua propagazione, è di fondamentale importanza in quanto essa determina la posizione ottimale del mandrino perforatore al fine di garantire un'elevata qualità del prodotto laminato e massimizzare la durata della punta.
Nonostante l'elevata esperienza dei produttori industriali, la conoscenza scientifica sull'effetto Mannesmann e sulle condizioni che lo determinano è notevolmente limitata. In generale, la letteratura tecnico-scientifica raccoglie numerosi studi sull'insorgere della frattura nei processi di deformazione in condizioni di lavorazione a freddo, c'è invece una sostanziale assenza di modellazione della rottura nel materiale in deformazione per quanto riguarda le lavorazioni ad elevata temperatura.
L'obiettivo di questo lavoro sta nello sviluppare un modello numerico in grado di riprodurre in modo affidabile le condizioni che industrialmente provocano la frattura per effetto Mannesmann nel processo di perforazione, mediante l'implementazione in un codice di calcolo di una legge di danneggiamento opportunamente calibrata sulla base del reale comportamento del materiale.
Mediante studi di carattere sperimentale, si dimostrato come la fase di solidificazione dell'acciaio dopo l'operazione di colata continua provochi una

forte differenziazione del materiale della billetta in termini di porosità e distribuzione delle diverse fasi che si riflette nel suo comportamento durante l'operazione di formatura. La lavorabilità del materiale in condizioni di processo è esaminata mediante prova di trazione ad elevata temperatura su provini estratti da billetta ottenuta per colata continua e osservazioni a microscopio sono svolte al fine di correlare la posizione dei campioni sulla billetta con le sue caratteristiche microstrutturali.
La caratterizzazione delle condizioni di frattura è possibile grazie all'utilizzo di un modello di danno secondo la formulazione di Lemeitre e l'identificazione dei parametri di danno dipendenti dal materiale è basata sull'uso di tecniche di analisi inversa in riferimento ai risultati sperimentali dei test di trazione a caldo. In particolare, una modifica alla legge di danno è introdotta al fine di descrivere correttamente le differenze nel comportamento del materiale nella sezione della billetta e considerare quindi l'effetto di porosità e distribuzione di fasi nello stato del materiale iniziale.
Al termine, il modello numerico sviluppato è validato mediante il confronto dei risultati da simulazione e fermi-macchina in impianto perforatore industriale in assenza del mandrino, che dimostra la bontà del modello per quanto riguarda la previsione del sito di frattura e della lunghezza del cono Mannesmann.

LIST OF FIGURES

LIST OF TABLES

CHAPTER 1

INTRODUCTION

1.1 CONTEXT

Seamless tubes are generally used in applications where safety plays a decisive role like sea or land oil-gas lines, pipe lines, oil rigs, and structural elements in the mechanical and automotive industry.
Seamless tube manufacturing is made up of several processes where an initial continuously cast cylindrical bar is transformed into a hollow part and then calibrated to the desired diameter and thickness.
Fig. 1.1 summarizes the first part of the manufacturing process. The main operations necessary to obtain the cylindrical bar are schematized. Steel scrap is charged and melted in the furnace, treated in the melting pot in order to

obtain the desired chemical properties and then continuously cast on a vertical or horizontal plant.

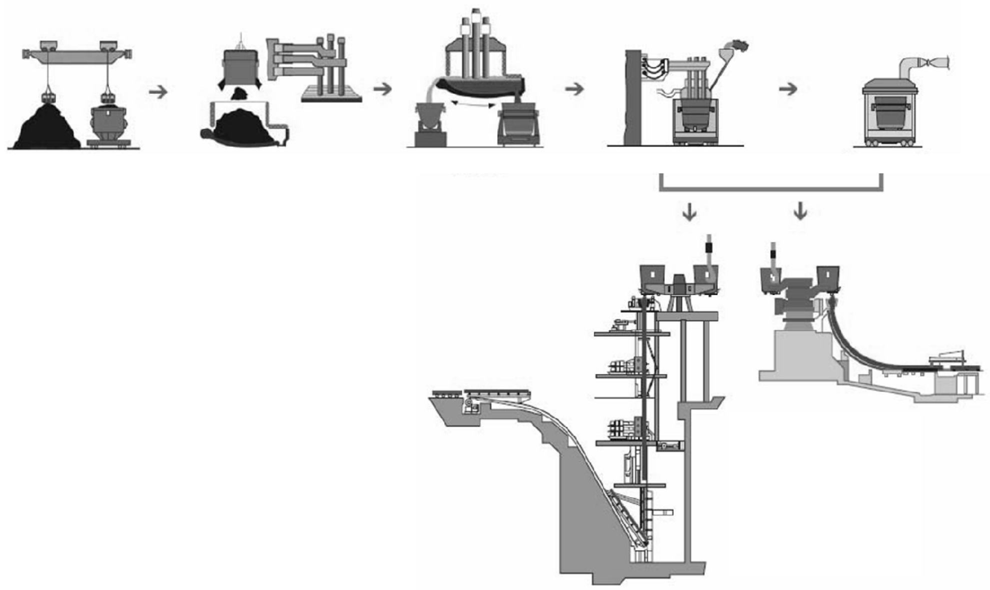

Fig. 1.1 Scheme of continuous casting processes for cylindrical steel billet (courtesy of XXXXXXXXX)

After casting, the cylindrical bar is heated up to 1250-1300 °C and maintained in a furnace until a uniform thermal condition is obtained. At this stage, it is ready for the necessary forming processes. Fig. 1.2 represents the forming chain that results in a seamless tube starting from the cylindrical bar.

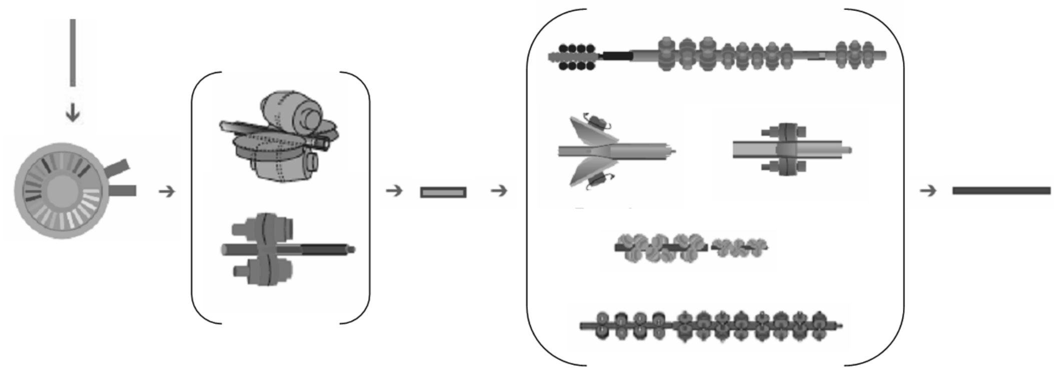

Fig. 1.2 Schematization of the main operation for seamless tube production (courtesy of XXXXXXXXX)

The first operation of tube forming is piercing which is industrially carried out using two different plant configurations named Mannesmann (with linear guides) and Diesher mill (with circular guides). When the hollow part comes out from the piercing mill, it undergoes several different rolling passes using different rolling mill configurations (pilger rolling, plug rolling, elongation pass, stretch reducing rolling, sizing and finishing cold operations) depending on the characteristics of the desired final part in terms of outer diameter and thickness.
This sequence of forming operations improves the dimensional and mechanical characteristics of the tubes compared to welding technology, as they are characterized by an elevated resistance to high pressure, obtained thanks to the fine and uniform microstructure granted by the process.
The piercing operation plays a decisive role in the final tube characteristics. In order to obtain a high quality final tube it is necessary to utilize a high quality hollow part, and for this reason, later on the piercing features will be treated in detail.

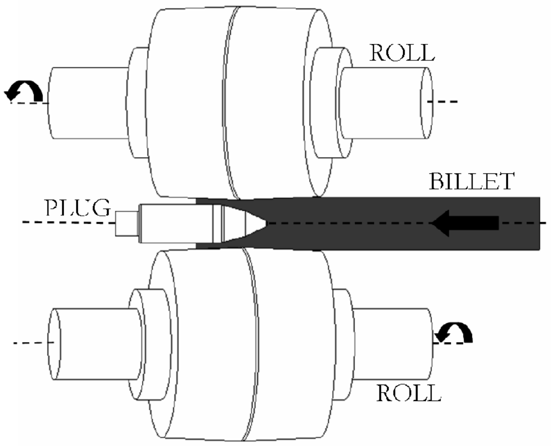

Fig. 1.3 The Mannesmann piercing scheme

Industrially, the continuously cast cylindrical billet enters the Mannesmann piercing mill at an initial temperature of 1250-1300°C. It passes through the gap of two skew conical rolls that have been accurately positioned in order to obtain the desired diameter reduction for the billet and its dragging towards the plug (Fig. 1.4).

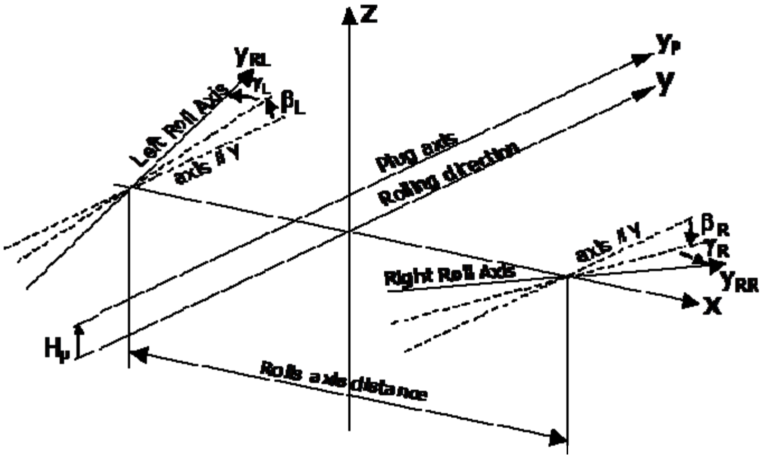

Fig. 1.4 Tools positioning parameters in the piercing mill

The particular geometry of the rolls and their inclination are at the basis of the phenomenon known as the Mannesmann effect that provokes a fracture along the longitudinal axis of the billet, thanks to the stress-strain state arising at the billet centre. In fact, the rolls action is responsible for a compressive state (C) that causes a secondary tensile component of tension (T) as schematized in Fig. 1.5.

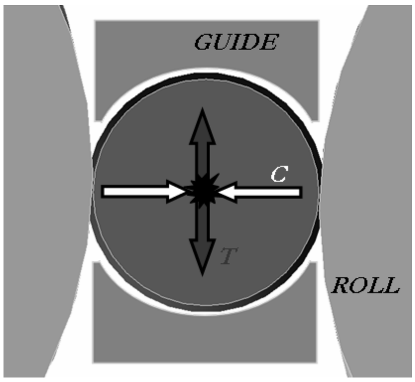

Fig. 1.5 The Mannesmann effect scheme

1.2 INDUSTRIAL-SCIENTIFIC PROBLEM

A fracture is usually not desired during forming operations, however in the case of tube piercing, the crack on the billet due to the Mannesmann effect is not noted as a defect but instead a fundamental aspect to take into account for a good process outcome.

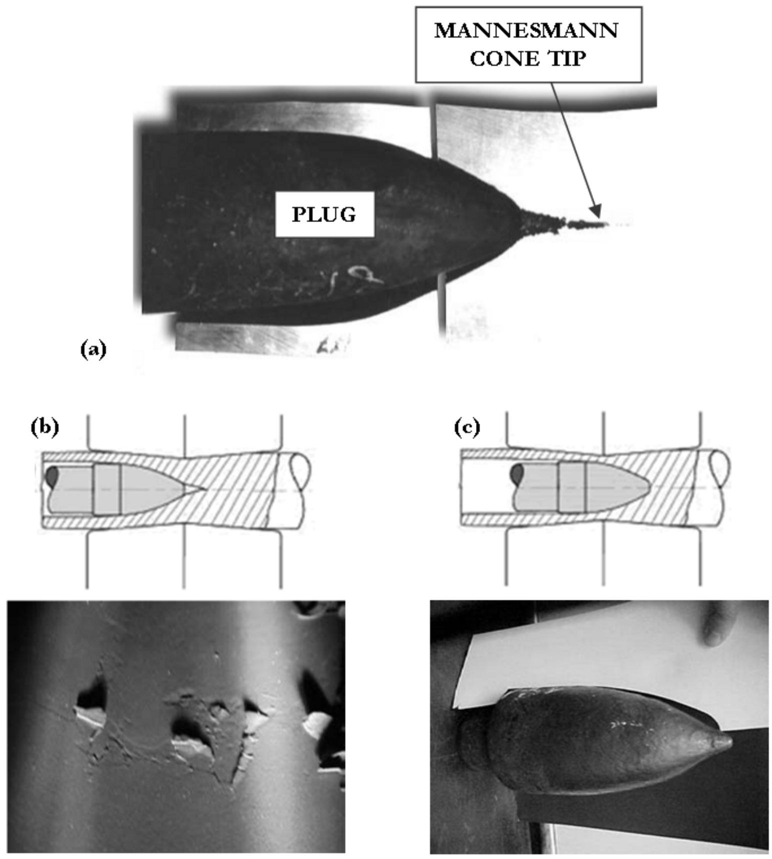

Fig. 1.6 Influence of the plug positioning (courtesy of XXXXXXXX)

The appropriate set up of the piercing operation depends on the position in which this internal feature initiates, since the plug acts as a mandrel enlarging an existing hole and not piercing directly the bulk material (Fig. 1.6a):

- If the distance of the plug from the billet is large, the internal surface of the crack will experience an excessive oxidation leading to defects in the final tube (Fig. 1.6b);

- if the fracture in the central part of the billet is not initiated when the plug pierces the material, the wear is excessive and the service life of the mandrel decreases significantly. (Fig. 1.6c).

Numerous process parameters affect the Mannesmann cone formation: tools geometry, kinematics, tools positioning, tube material and dimension. Even if the Mannesmann piercing operation dates back to over a hundred years ago, as soon as new forming conditions are adopted, the set up of the mill is still based on experience and trials.

In view of these observations, two fundamental aspects can be distinguished regarding the Mannesmann fracture formation:

- the *industrial requirement*; the position of the plug on the piercing mill has to be set in relation to the central crack formation. For this reason, a reliable and quick method able to predict the Mannesmann fracture position can aid the tube manufacturer and help avoid expensive trials (tube steel losses and damaged plugs due to incorrect axial positioning);
- a *scientific problem*; the crack due to the Mannesmann effect initiates, in particular, tri-axial conditions typical of piercing operations. Its prediction requires an in-depth investigation of the stress-strain evolution on the billet coupled with an extensive investigation of the material workability.

CHAPTER 2

BACKGROUND STUDY AND LITERATURE REVIEW

2.1 INTRODUCTION

The analysis of the problem is carried out starting from the main concept of workability and focusing attention on the damage and fracture of the materials during metal forming processes.
Implementation of damage models on numerical simulations to predict material failure during forming is widely diffused in cold conditions while few applications can be found at elevated temperature; technical-scientific literature contents are summarized.

2.2 MECHANICAL FAILURE

2.2.1 Workability and fracture of metals

Technical literature contains many definitions of the term "workability". Regarding metalworking processes, it can be resumed as the relative ease with which a metal can be shaped through plastic deformation (i.e. the maximum amount of deformation that metal can withstand in a particular process without failure) and it is often synonymous of ductility [1,2]. It is a complex property that depends simultaneously from material characteristics (i.e. mechanical strength, rheology, hardness, strain hardening) and process parameters determining the stress system (Fig. 2.1).

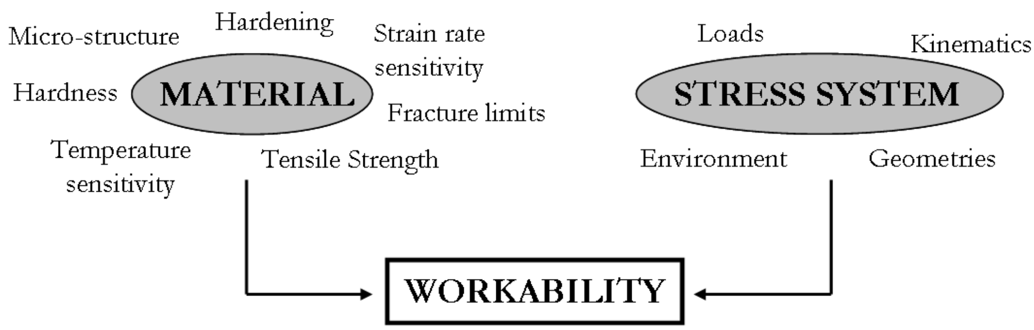

Fig. 2.1 Workability definition

In order to properly design a metal forming operation, it is necessary to understand the failure behavior of the part material under the particular working condition.
In order to evaluate the potential for fracture of a material during a particular process, it is necessary to combine a laboratory test with a fracture criterion: the first establishes the ductility of the material under standard conditions (i.e. tension test, compression test, torsion test, …,); the second extends the results of workability test to the stress and strain conditions existing in the deformation process being examined..
From the engineer's point of view, there are two types of fractures, ductile and brittle, with respect to the amount of plastic deformation (stored energy) that

the material undergoes before rupture. Only the ductile fracture will be considered for now since this is the main type of failure that occurs in metalworking operations and almost the only one that characterized the deformations performed at elevated temperatures.
The micro-mechanics of ductile fracture is made up of three different stages:
- voids nucleation, usually at the boundary of a second phase particle or inclusion (stress controlled process);
- voids growth, in terms of increasing volume and changing shape due to the deformation of the surrounding plastic matrix (strain controlled process);
- voids coalescence, due to the interaction between neighboring big holes, through which the macroscopic fracture starts and propagates (strain controlled process).

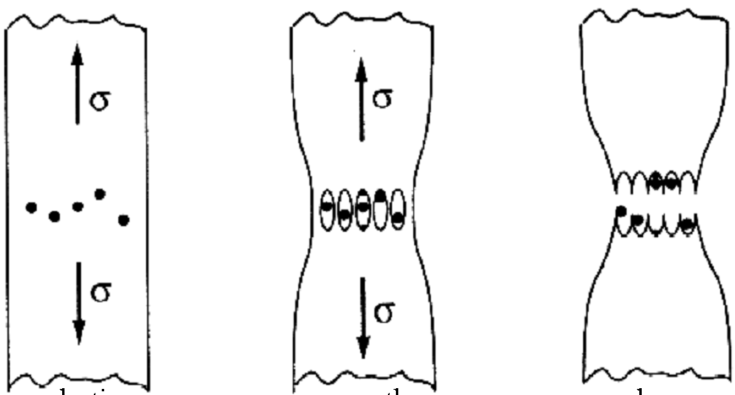

Fig. 2.2 Stages of ductile fracture

2.2.2 Role of stress triaxiality on material failure properties

There are numerous studies in technical literature regarding the dependency of ductile fracture on the multi-axial aspects of the state of stress: McClintock [3], Rice and Tracey [4], Oyane [5] and Atkins [6] are only some of the researchers that demonstrated through experiments, empirical routes or continuum mechanics, that there is a strong influence of the hydrostatic stress on the fracture limit of ductile materials such as steel or aluminum.
The concept of triaxiality is introduced to represent the multi-axial character of a state of stress and takes into account its influence on the final response of the material:

$$\frac{\sigma_H}{\overline{\sigma}} \quad \text{stress triaxiality;} \tag{II.1}$$

$$\sigma_H = \frac{\sigma_1 + \sigma_2 + \sigma_3}{3} \quad \text{hydrostatic stress;} \tag{II.2}$$

$$\overline{\sigma} = \frac{1}{\sqrt{2}}\sqrt{(\sigma_1 - \sigma_2)^2 + (\sigma_1 - \sigma_3)^2 + (\sigma_2 - \sigma_3)^2} \quad \text{equivalent stress} \tag{II.3}$$

σ_i, i=1-3 principal stress components.

It was demonstrated that, together with the strain intensity, the triaxiality plays a fundamental role on the crack formation on ductile materials, usually equivalent strain at fracture is taken as a good estimation of the ductility under the considered stress condition. Performing tensile tests on different geometries notched specimens in order to realize different value of triaxiality, it is provable how an increasing of the triaxiality provokes a decreasing of the equivalent strain at crack initiation.

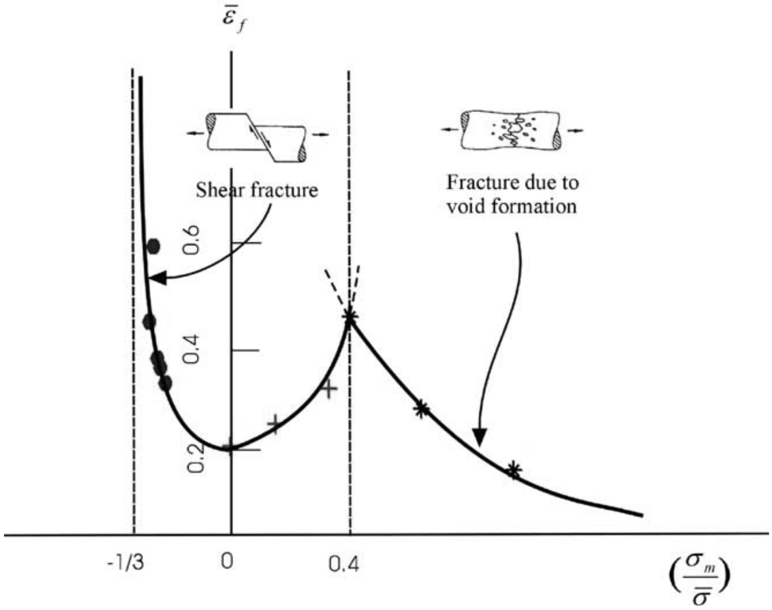

Fig. 2.3 Dependency of equivalent strain at fracture on the stress triaxiality [9]

This field was deeply investigated by Bao et al. [7-9] through numerical and experimental methods and the following diagram (Fig. 2.3) represents a resuming of their works. Depending on the triaxiality amount, the material under deformation can reach failure in different modes (shear fracture for low triaxiality and fracture due to void formation when high triaxiality values are performed); in addiction they proposed a lower limit in the triaxiality value (equal to -1/3), below which the hydrostatic stress has not effects on the strain at fracture (confirmed by experiments).

2.2.3 Fracture criteria

The main purpose of a fracture criterion is to predict the initiation site and the level of deformation at which the crack will occur in a material during a particular metalworking operation. The concept of "damage" is introduced and is defined as the deterioration of the material capability to carry load. It develops in the microstructure when non-reversible phenomena such as microcracking and debonding between matrix and second phase particles and microvoid formation takes place. From a general point of view, a fracture criterion should represent the material degradation due to the voids formation and it should detect the precise amount of damage causing the material failure. The objective is to establish a significant parameter that describes the amount of damage in the material during deformation. This particular parameter reaches its critical value when fracture occurs.
When a fracture criterion is chosen, the critical value of its significant parameter is determined experimentally from a workability test (under standard conditions) and represents the condition at which a fracture occurs also in the real process to analyze.
Nowadays, damage models are frequently implemented into numerical codes in order to predict material failure and optimize processes and parts aiding their engineering.
Damage models can be distinguished into two main categories, depending on the approach used to derive their formulation and they are applied into the code:

1. uncoupled damage models, in which damage does not directly affect the material properties but it represents a post-processing calculation of the finite element analysis.
2. coupled damage models, in which the material degradation due to the deformation (and therefore to the voids formation) is progressively

taken into account and used to reduce the material strength. The material resistance for every calculation depends on the amount of damage.

Fig. 2.4 and 2.5 report the flow procedure at the basis of a finite element analysis in both cases of uncoupling and coupling damage approaches for fracture description.

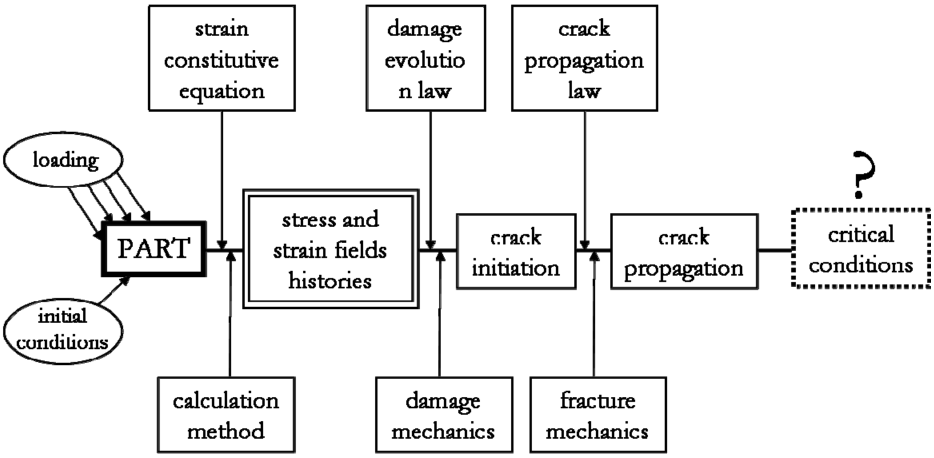

Fig. 2.4 Scheme of uncoupled calculation of strain crack formation

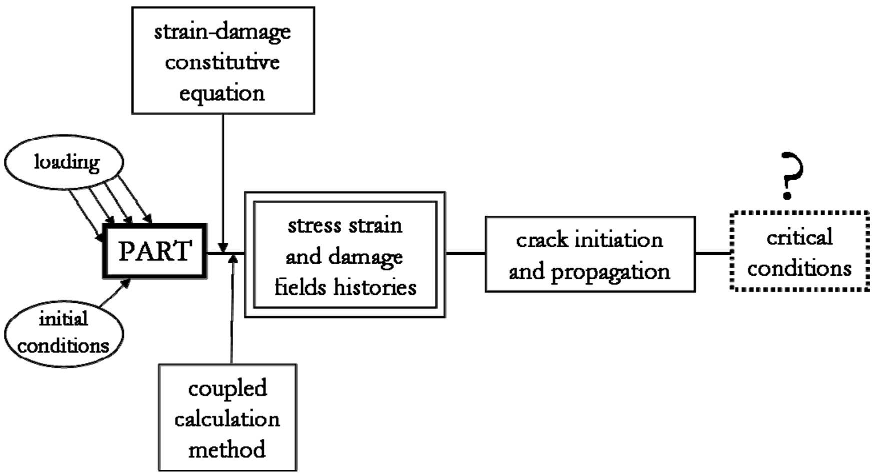

Fig. 2.5 Scheme of calculation for coupled strain and damage

Fig. 2.6 summarizes the meaning of coupling/uncoupling in the material behavior in terms of elastic-plastic properties when a damage model is implemented into numerical simulation. Usually, for metallic materials, a threshold strain (ε_{th}) exists over which the difference between damaged and integral material properties becomes evident; while the damage increases, the material strength (in terms of flow stress) is progressively decreased due to the voids formation.

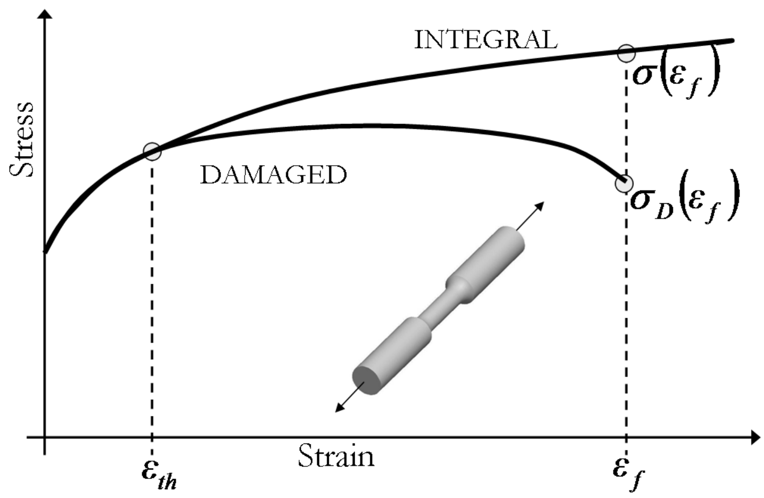

Fig. 2.6 Coupling and uncoupling damage

Uncoupled approaches include energy-based and damage models deriving from the micromechanics of voids formation. Coupled approaches include criteria based on porosity and models deriving from the Continuum Damage Mechanics field (a few examples are reported in Tab 2.1).

UNCOUPLED APPROACHES		**COUPLED APPROACHES**	
ENERGY-BASED MODELS	VOIDS GROWTH MICRO-MECHANICS	POROSITY-BASED MODELS	CONTINUUM DAMAGE MECHANICS
Cockroft & Latham Brozzo Freudenthal	McClintock Rice & Tracey Oyane	Gurson Tveegard & Needleman	Lemaitre

Tab. 2.1 Damage models categories

2.2.3.1 Energy-based fracture criteria

Damage models included in this category are also referred to as empirical because they were derived generally from observations on specific forming processes. Normally, the implementation of these kind of approaches into numerical simulation is simple and fast but they can give a good fracture prediction in the cases similar to which they are derived; when the state of stress or strain history is too different from the reference, these models cannot predict fracture accurately.
Cockcroft and Latham [1] proposed probably the most diffused damage model in metal-forming applications:

$$D = \int_0^{\varepsilon_f} \sigma_1 d\varepsilon \qquad \text{(II.4)}$$

The damage variable D in (II.4) represents the internal plastic energy necessary to deform the material until fracture strain ε_f is reached. The fundamental role of the tensile stress (represented by the first stress principal component) on the crack formation is at the basis of the expression.
In view of the limited range of situations in which the Cockcroft and Latham model gives a reliable fracture prediction, a normalized version was introduced in order to improve its capabilities when the state of stress is not purely tensile:

$$D = \int_0^{\varepsilon_f} \frac{\sigma_1}{\bar{\sigma}} d\bar{\varepsilon} \qquad \text{(II.5)}$$

Freudenthal proposed a different formulation than Cockcroft and Latham based on the plastic work of deformation calculated by using equivalent stress in place of the first principal component (generalized plastic work) [10]:

$$D = \int_0^{\varepsilon_f} \bar{\sigma} d\bar{\varepsilon} \qquad \text{(II.6)}$$

The last energy-based model presented here was proposed by Brozzo et al.

[11]. It is characterized by the explicit dependency of both levels of the first principal stress component and the hydrostatic stress by means of an empirical modification of the Cockcroft and Latham criterion:

$$D = \int_0^{\varepsilon_f} \frac{2\sigma_1}{3(\sigma_1 - \sigma_H)} d\bar{\varepsilon} \qquad \text{(II.7)}$$

2.2.3.2 *Damage criteria based on void growth*

Numerous experimental results show that ductile fracture in metals is due to voids nucleation, growth and coalescence, as anticipated in section 2.2.1.
McClintock [3] was one of the first exponents of the damage modeling through this approach. In his most famous work, the author modeled ductile failure initiation assuming the presence of micro-voids in a plastic material and studying what happens to a single long cylindrical cavity in the matrix in terms of size and shape when a state of stress is applied. In spite of a simplified representation of the single void growth and the states of stress and strains, the model was able to describe the failure condition in numerous experimental conditions and made possible many observations concerning triaxiality, strain hardening and stress/strain history influences on ductile fracture.
II.8 represents an expression usually implemented into commercial numerical codes derived from McClintock's studies. It describes the damage evolution on a section of material characterized by a plane state of stress according to one of the author's symmetry hypothesis (see scheme in Fig. 2.7 referred to the simplified stress state assumption).

$$D = \int_0^{\varepsilon_f} \left\{ \frac{2}{\sqrt{3}(1-n)} \sinh\left[\frac{\sqrt{3}(1-n)}{2} \frac{\sigma_a - \sigma_b}{\bar{\sigma}} \right] + \frac{\sigma_a - \sigma_b}{\bar{\sigma}} \right\} d\bar{\varepsilon} \qquad \text{(II.8)}$$

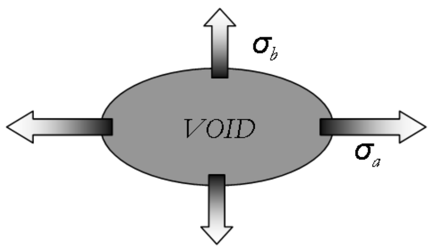

Fig. 2.7 Scheme of the simplified state of stress of the McClintock model

McClintock's work represented a milestone on fracture modelling based on voids growth. Improvements to this theory were followed thanks to studies carried out by Rice and Tracey [4]. Driven by McClintock's previous research about an isolated spherical void in a remotely uniform stress and strain rate field, they proposed a more realistic view of ductile fracture considering the role of triaxiality and the interaction and unstable coalescence of neighboring voids into the criterion (Fig. 2.8). Equation II.9 represents a common formulation of the Rice and Tracey criterion implemented into a commercial numerical code for forming process simulation, where *A* is a material dependent constant that has to be determined experimentally:

$$D = \int_0^{\varepsilon_f} A \exp\left(\frac{3\sigma_H}{2\bar{\sigma}}\right) d\bar{\varepsilon} \qquad \text{(II.8)}$$

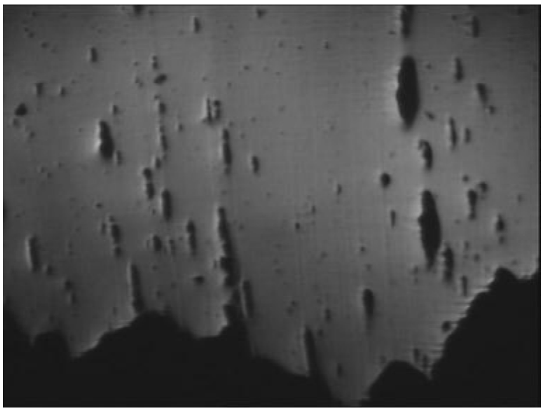

Fig. 2.8 Coalescence of voids in tensile specimen necking region

Hankock and Mackanzie [12], following the previous works of McClintock and Rice and Tracey, focused their investigation on the effects of stress system orientation with respect to the rolling direction of the material (anisotropic behavior of directional steels) and of triaxiality on ductility. Important conclusions were reached by the authors:

- a failure criterion must involve a certain minimum amount of material which is characteristic of the scale of physical events leading to local failure; a fracture condition reached in a single point is not sufficient for failure initiation in a ductile material matrix;
- particles on the material matrix (i.e. carbides or other precipitates) are strong influences on the coalescence procedure of big voids and therefore the fracture evolving;

- the mechanism of failure initiation is affected by the reciprocal orientation of matrix grains and stress system (i.e. differences on fracture behavior when testing tensile samples aligned to rolling or transverse direction).

Finally, Oyane criterion [5, 13] is the last void growth model presented here. It was derived considering the three stages of ductile fracture under the issue of the theory of plasticity for porous materials:

$$D = \int_0^{\varepsilon_f} 1 + B\frac{\sigma_H}{\overline{\sigma}} d\overline{\varepsilon} \tag{II.9}$$

where B is a material constant. Oyane et al. tested the model for the prediction of failure during two different forming operations (upsetting and indirect extrusion) verifying its capabilities when different states of stress (in terms of triaxiality) were deforming the material. Following applications confirmed how this model is suitable for many common situations in forming processes and for this reason it is incorporated into several specific numerical commercial codes.

2.2.3.3 Porosity-based ductile fracture criteria

Void fraction and porosity concepts are at the basis of this approach through which it is possible to perform a coupled analysis for the material damage characterization.

Gurson was probably the pioneer of the porosity-based damage modelling. In his most famous work [14] he considered the material as a porous medium where the influence of nucleated voids on the stress/strain state and plastic flow cannot be neglected. Nucleation and void growth were being modelled and the second stage of fracture (growth) was recognized as the dominant one on ductile crack initiation. The assumption that micro-voids do not interact is a simplification linked to the analytical procedure used. It also represents the main limit of the model proposed by Gurson which did not permit the modelling of the final stage of void growth, which is when coalescence of voids occurs by localized straining due to internal necking of the intervoid matrix. In order to take in to account the evident effect of the coalescence of adjacent voids on crack initiation and propagation, Tvergaard and Needleman [15, 16] introduced an empirical modification of the Gurson yield function.

Finally, the porosity-based approach is represented by the so called GTN

model (Gurson - Tvergaard - Needleman). It is founded on the hypothesis that micro-mechanical features at the basis of ductile fracture in metal, void nucleation and growth, can be macroscopically described by extending the Von Mises plasticity theory to cover the effects of porosity occurring in the material.
A scalar damage quantity, the void volume fraction *f*, defined as the average ratio of the voids volume to the total volume of the material, is the primary concept necessary for the porosity description and is introduced as an internal variable to characterize the damage. Following the GTN model, the analytical formulation usually implemented into numerical codes is briefly reported.
Nucleation (regulated by the equivalent plastic strain rate) and growth (dependent on the plastic volume dilatation rate) are two contributions of void fraction evolution:

$$\dot{f} = \dot{f}_{nucleation} + \dot{f}_{growth} \qquad \text{(II.10)}$$

$$\dot{f}_{nucleation} = A\dot{\bar{\varepsilon}}_{p} \qquad \text{(II.11)}$$

$$\dot{f}_{growth} = (1-f)\dot{\varepsilon}_{p,ii} \qquad \text{(II.12)}$$

With $f(t_0)=f_0$ represents the initial void fraction.
Fracture description is done by void fraction f^*:

$$f^* = \begin{cases} f; & f \le f_C \\ f_C + K(f - f_C); & f > f_C \end{cases} \qquad \text{(II.13)}$$

Where f_C is the critical void fraction at which fracture initiates, K is a material dependent parameter representing an accelerating factor for the propagation fracture stage.
The coupling between material strength and damage is realized by extending the classical yield condition according to Von Mises plasticity theory and introducing the void volume fraction (eq. II.14):

$$\phi = \frac{3\sigma_{ij}\sigma_{ij}}{2\bar{\sigma}} + 2q_1 f^* \cosh\left(q_2 \frac{3\sigma_H}{2\bar{\sigma}}\right) - \left[1 + (q_3 f^*)^2\right] = 0 \qquad \text{(II.14)}$$

Where q_1, q_2, q_3 are material dependent parameters.
Many successful studies have been carried out on the basis of the GTN model, confirming its capability in damage evolution and ductile fracture prediction in metallic materials. Some observations related to its application in the metal forming field will be given in sections later on.

2.2.3.4 Continuum damage mechanics approach for ductile fracture

Continuum Damage Mechanics (CDM) approaches the failure using continuum concepts and, the constitutive equations for the damaged material are written taking into account the specific micro-mechanism of failure.
The reference in this field is represented by Lemaitre's work: he proposed the constitutive equations for a ductile damaged material [18-21] starting from the "effective stress" concept proposed by Kachanov [17]. In this context, a brief presentation of this theory is given, focusing the attention on the applicability aspects avoiding the rigorous analytical formulation.

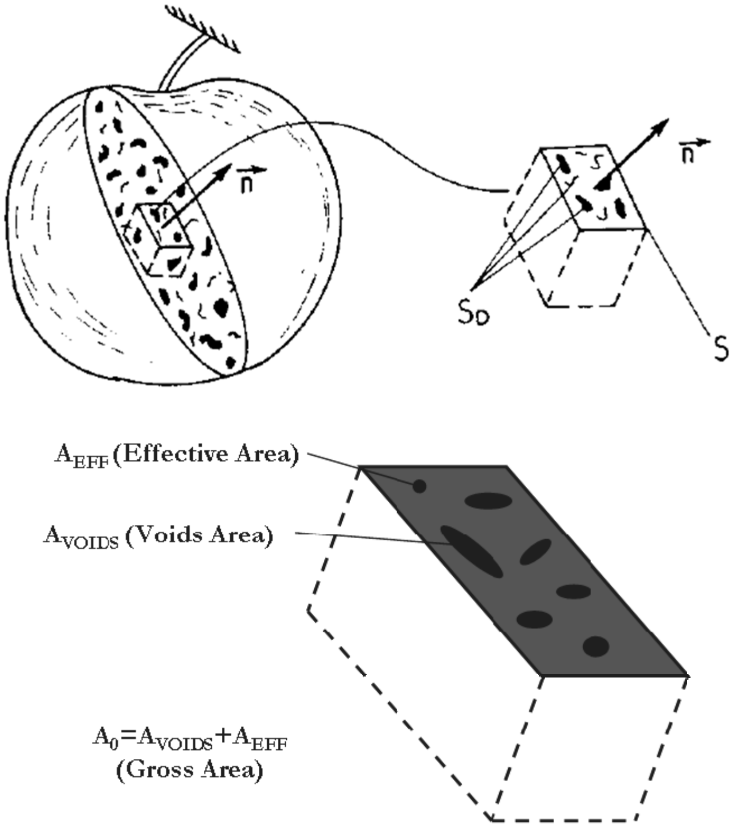

Fig. 2.9 Representative volume element [18]

Considering a damaged body, a reference volume element (RVE) is the volume at micro-scale of a size large enough to contain many defects and small enough to be considered as a material point in the mechanics of continua. Referring to the RVE schematization in Fig. 2.9, the damage variable D can be defined as:

$$D = \frac{A_{VOIDS}}{A_0} = 1 - \frac{A_{EFF}}{A_0} \tag{II.15}$$

Let A_0 the overall section of this element, A_{EFF} the effective resisting area and A_{VOIDS} the area covered by voids (or more in general defects on the material matrix).

Undamaged material corresponds to $D=0$ while the rupture of the element corresponds to a critical value $D=D_C$ ($0.2 \leq D_C \leq 0.8$ for metals).

Once the damage variable is available, it is possible to calculate the effective stress using the nominal stress σ calculated as the density of force with regard to the gross area A_0:

$$\sigma_{EFF} = \frac{\sigma}{1-D} \tag{II.16}$$

Considering effective values (area, stress, elasticity, ..) means to assume a coupled damage approach and take into account the effect of progressive degradation on the material properties due to a damage process that is increasing the size of the damaged section in the RVE (A_{VOIDS}) to the detriment of the resistant area (A_{EFF}).

Lemaitre based his studies on the fundamental hypothesis of strain equivalence: "every strain behavior is represented by constitutive equations of the undamaged material in the potential in which the stress is simply replaced by the effective stress". From the hypothesis follows that the constitutive equations of a damaged material are the same as those of the virgin material with no damage in which the nominal stress is simply replaced by the effective stress. An example of its application concerning the linear elasticity equation is reported:

$$\varepsilon = \frac{\sigma}{E} \qquad \text{undamaged material}$$

$$\varepsilon = \frac{\sigma_{EFF}}{E} = \frac{\sigma}{(1-D)E} \qquad \text{damaged state}$$

Lemaitre, by first defining what are called damage strain energy release rate $-y$ (II.17), and potential of dissipation φ (II.18), was then able to derive constitutive equations of dissipative variables. Only the isotropic formulation for damage is reported here, refer to [20] for more details concerning the more general anisotropic case:

$$-y = \frac{\bar{\sigma}^2}{2E(1-D)^2}\left[\frac{2}{3}(1+\nu)+3(1-2\nu)\left(\frac{\sigma_H}{\bar{\sigma}}\right)^2\right] \qquad \text{(II.17)}$$

$$\varphi = \frac{S_0}{(s+1)}\left(\frac{-y}{S_0}\right)^{s+1}\dot{\bar{\varepsilon}}_p \qquad \text{(II.18)}$$

Where the damage strength S_0 and the damage exponent s are material and temperature dependent parameters. The quantity in square brackets in eq. II.17 is usually called triaxiality function R_V in view of its stress triaxiality factor dependency. $\dot{\bar{\varepsilon}}_p$ represents the accumulated plastic strain rate.
The damage evolution law derives from the potential of dissipation by:

$$\dot{D} = -\frac{\partial\varphi}{\partial y} = \left(\frac{-y}{S_0}\right)^{s}\dot{\bar{\varepsilon}}_p \qquad \text{(II.19)}$$

Lemaitre defined a strain threshold value ε_{th} above which the damage that starts to grow is a material property to define experimentally.
In view of the square of stress triaxiality term in triaxiality function, there is no difference between material degradation under tensile or compressive state of stress. In order to take into account what is known as the crack closure effect on damage evolution, or rather the decrease of the damage rate due to a compressive state of stress, the expression in eq. II.19 was used only for positive values of stress triaxiality. For negative values of stress triaxiality, the formulation of eq. II.20 was proposed in order to consider the effects induced by a compressive state of stress into the damage evolution.

$$\dot{D} == \left(\frac{-h_C y}{S_0} \right)^s \dot{\bar{\varepsilon}}_p \qquad \text{(II.20)}$$

The parameter h_C is the reducing factor which takes into account the crack closure effects and is set equal to 0.2, according to [21].
Similar to the other approaches for fracture description, this model also requires the condition that corresponds to failure initiation which is fixed by an experimentally defined value of damage D_C (corresponding to a critical value of damage energy release rate $-Y_C$).
Recently, in the context of CDM and starting from the work of Lemaitre, Bonora proposed a nonlinear model for ductile fracture developed from experimental observations [22]. A general nonlinear damage dependency from plastic deformation was established when a new exponent that determines the shape of the damage evolution with plastic strain was introduced. Investigations made by the author [23, 24] demonstrate the geometry transferability of the damage parameters definition in predicting failure initiation under multi-axial state of stress loading conditions.

2.3 DAMAGE MODELLING AND FRACTURE PREDICTION IN METALWORKING PROCESSES

Numerical simulation has become a very useful tool during the forming operation development and optimization stages. Fracture criteria implementation can be used to investigate the critical conditions in which the formed part material reaches the crack onset.
Usually, from the industrial point of view, fracture arising is a negative aspect strongly avoided since cracks are the worst defects on forged parts. Actually, there are some situations in which a particular fracture type is necessary to realize in the forming operation in order to obtain a good final part. The main example of this category is Mannesmann piercing during the seamless tube production that will be will be presented later on in detail.
Applications on forming context coming from technical-scientific literature regarding different approaches to fracture are reported in this section.
Nowadays, it is common for researches to think that there is no unique and universal model that can describe all fracture conditions: a damage model can give the best and most reliable prediction for a certain operation and at the same time the worst for a different one, depending on the process condition

(i.e. deformation history, state of stress and triaxiality, material rheology in terms of temperature and strain rate sensitivity).
There are many publications in literature that evaluate the capabilities of different damage models applied on certain forming operations [25-50]. Most applications refer to forging components or sheet metal forming at room temperature and very few examples can be found regarding the fracture prediction in hot steel working operations.
Cockcroft & Latham, Oyane and Brozzo are the the most frequently used damage models in bulk metal forming simulation when no particular accuracy is needed. Some applications at room temperature are reported in [25-29]. An analysis of the literature leads to the assumption that this kind of models represents a useful tool for the engineer when the primary need is to quickly pick out the fracture site during the forming operation. An important advantage using these simple models is the ease with which they can be calibrated and implemented into the numerical model (in general few simple mechanical tests are sufficient to determine the few necessary material parameters). On the other hand, they do not give a good prediction of damage evolution in relation to the other variables, they cannot be applied for example to different states of stress [30] and, in addition, they are not able to localize damage distribution in sheet forming conditions [31].
If an accurate prediction of damage and fracture are required under a forming condition, a micromechanical based and most of all a coupled approach to damage modeling are necessary. The literature available suggests that Gurson based models [33-37] and Continuum Damage Mechanics [38-47] are the most proper ways to describe ductile fracture behavior.
Micromechanical modelling of damage requires a longer and more detailed calibration phase than the use of empirical-energy based criteria. In general, it is necessary to identify numerous material dependent parameters. Inverse analysis techniques on tensile test results are usually the typical tools for this kind of determination [33-35]. Many applications are present in technical literature confirming the damage prediction capability of models based on void growth and porosity. Komori [36] compared different approaches to fracture on modeling the chevron crack formation in drawing: Gurson and Oyane criteria resulted the most suitable for the reproduction of crack initiation and propagation (Fig. 2.10).

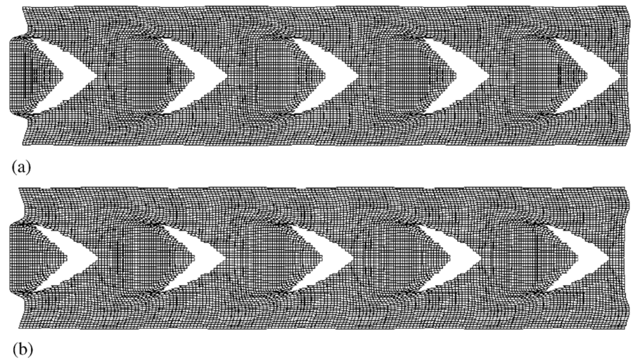

Fig. 2.10 Chevron cracks in drawing [36]

Uthaisangsuk et al. [37] applied the Gurson model to the investigation of formability in sheet metal forming and the numerical prediction was successfully compared to an estimation obtained through a forming limit diagram. Fig. 2.11 shows the results of this study in terms of load/displacement estimation in hot expansion test.

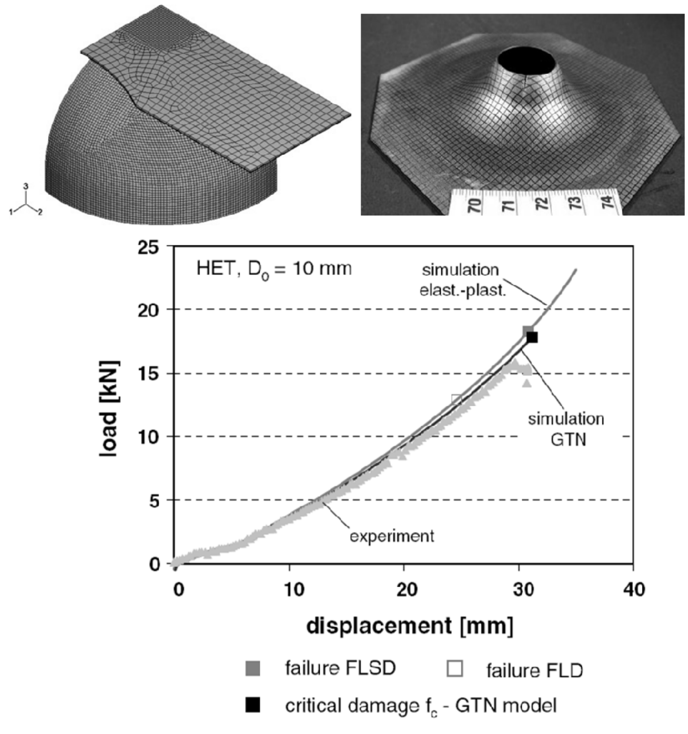

Fig. 2.11 Fracture in sheet metal forming [37]

Even if Continuum Damage Mechanic (CDM) dates back to many years ago, there has been a recent increase of interest on the application of this approach to the modeling of fracture in metal forming context. Just like the void growth based criteria, the implementation of these damage models typology into the numerical code requires a more expensive procedure if compared to the widely used energy-based ones. On the other hand, not only is the description closer to the real physical phenomena coming from the coupling between damage and material mechanical properties, Continuum Damage Mechanic avoids the investigation at the micro-scale. For instance, an accurate determination of voids fraction evolution is not necessary and their calibration is a little bit easier than the void growth based ones. According to continuum concepts, material damage characterization is determinable transposing mechanical considerations valid at the structure scale level to the macro-scale [20, 21].
Many successful applications of the Lemaitre approach can be found in technical literature, mainly forming operations at room temperature.
Hambli et al. predicted fracture in sheet metal forming. In particular, damage was modeled during the blanking (Fig. 2.12) [38] and bending [39] operations and the authors proposed an alternative procedure based on micro-hardness measurements for the model calibration in order to describe the fracture condition for sheet material in general [40].

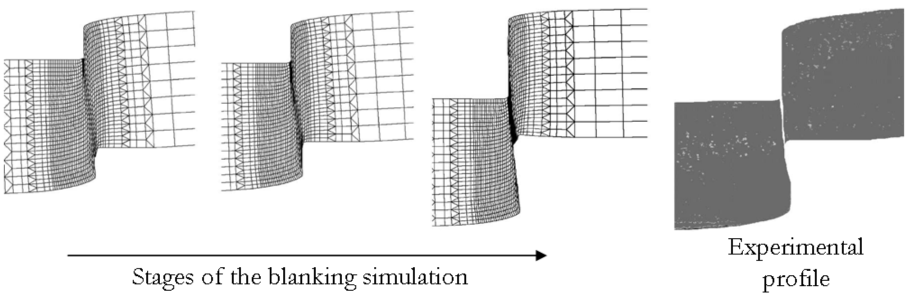

Fig. 2.12 Prediction of fracture in blanking using the Lemaitre damage model [38]

A very accurate analytical formulation of damage laws according to the Lemaitre theory was proposed by Andrade Pires et al. [41, 42]. Material dependent damage parameters were taken from previous works, fracture was modelled for various states of deformation deriving from different forming process conditions. Authors compared the computational results and experimental ones demonstrating the capabilities of the calibrated model to predict damage evolution during the tensile test of a notched bar (Fig. 2.13a), the upsetting of a tapered sample and the backward extrusion operation (Fig.

2.13b).

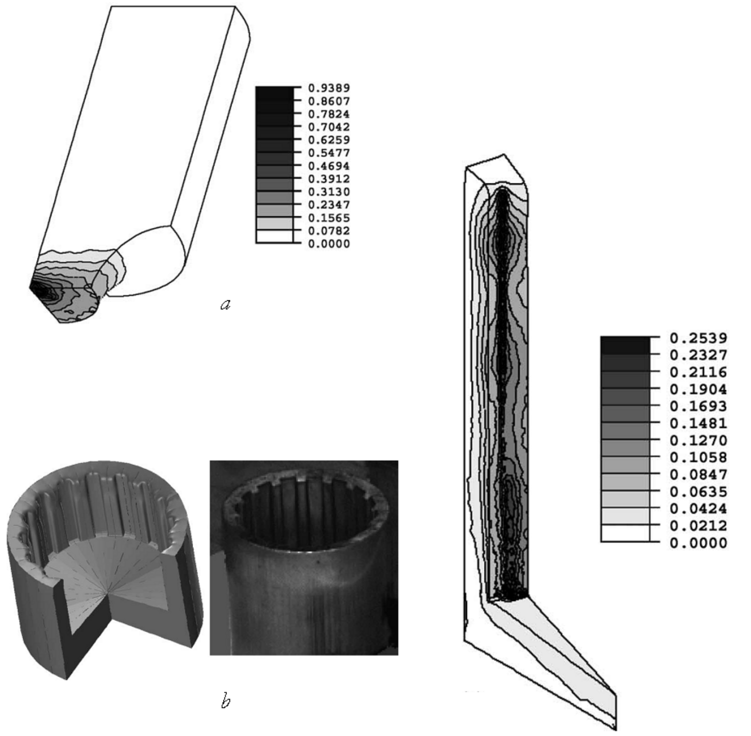

Fig. 2.13 Damage prediction in tensile test sample and backward extruded part [42]

Following the same analytical formulation of Andrade Pires et al., Cesar de Sà et al. [43, 44] modelled the fracture initiation in sheet metal forming conditions. In particular, Fig. 2.14 reports the main result coming from what is called "non-local gradient model" which authors obtained by modifying the standard Lemaitre theory (local model). The Gradient model seems to solve one of the main problems when fracture is modelled, especially in sheet forming conditions, that is mesh size dependency. The numerical prediction of force/displacement curve during sheet blanking in Fig. 2.14 confirms the very low mesh size influence if the new proposed approach is adopted.

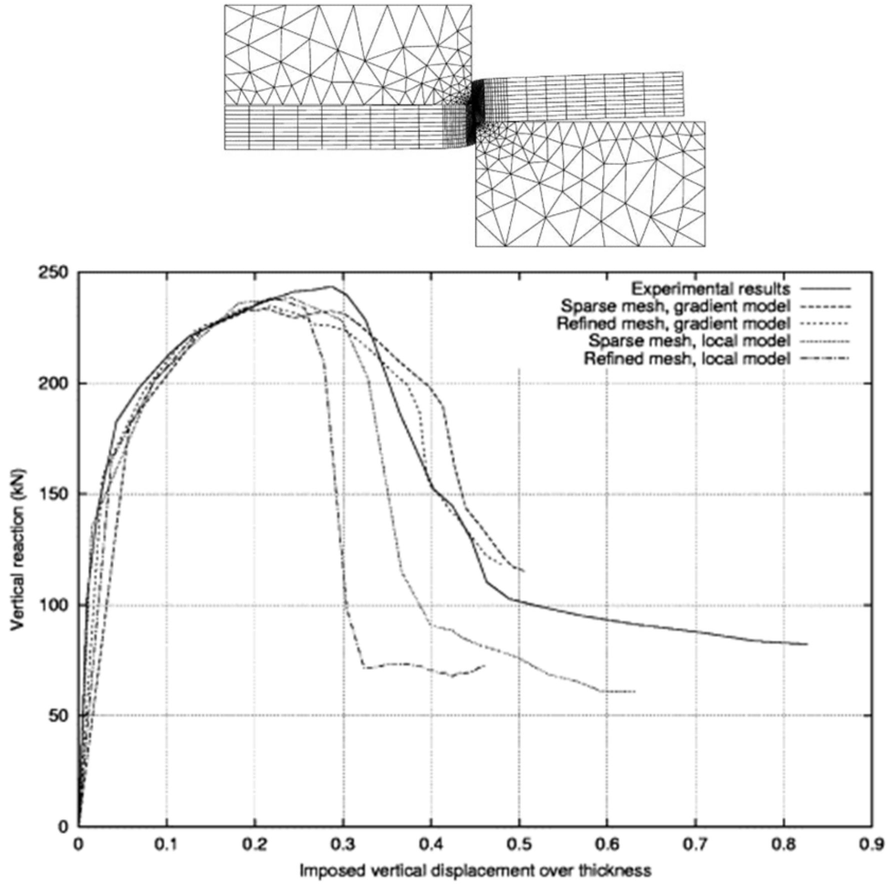

Fig. 2.14 Comparison between the local and gradient model in blacking simulation [44]

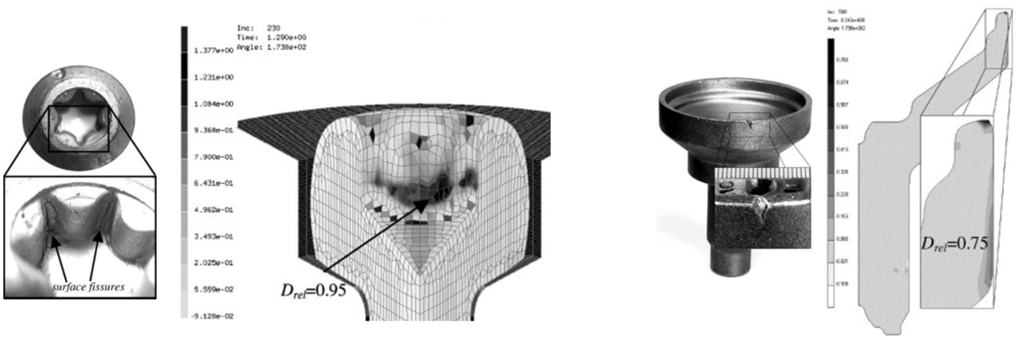

Fig. 2.15 Damage prediction in cold and warm forged parts implementing the effective stress model [45,46]

One of the few examples regarding fracture prediction in a warm or hot process condition is reported in Fig. 2.15 and refers to the work of Beherens and Just [45,46]. The authors proved the applicability of the Continuum Damage Mechanics approach on the numerical simulation of real industrial forging operations, calibrating the damage model using hot tensile and compression tests.
A very particular and successful application of the Lemaitre approach was given by P. O. Bouchard et al. [47] for modelling the self-pierce riveting operation (Fig. 2.16). In the riveting operation, two different sheets are fracturing, different fracture conditions were predicted depending on the material chosen for each part realizing the joint.

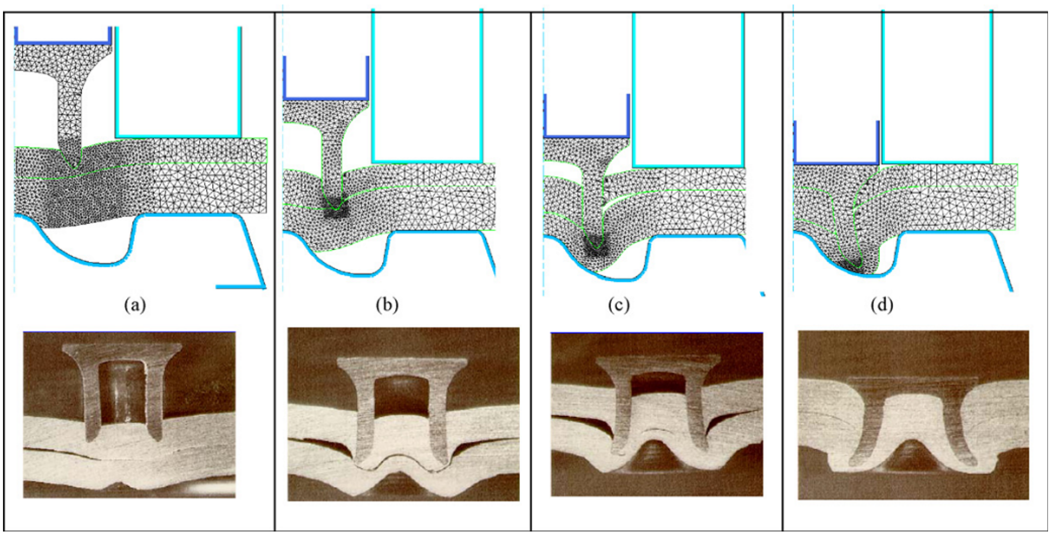

Fig. 2.16 Fracture modelling in self-pierce-riveting using the Lemaitre damage model [47]

There are very few publications in technical and scientific literature concerning damage modelling at an elevated temperature condition. The fundamental aspect that distinguishes hot condition approaches to fracture to room temperature ones is that the calibration of the model needs more accuracy in view of numerous phenomena that start influencing material behaviour when temperature increases (i.e. micro-structural changes, strain rate and temperature sensitivity of the flow properties).
Experimental and numerical procedures in [48, 49] are examples of a Rice and Tracey model calibration and an investigation of thermo-mechanical conditions leading to fracture at elevated temperatures.

Based on what has been reported in this paragraph, fracture modelling is widely used in cold conditions and there are many applications. At the same time, it is evident that a more accurate and profound understanding of the mechanisms of damage initiation and propagation at elevated temperature is necessary in order to improve their numerical modelling.

2.4 MANNESMANN PIERCING PREVIOUS STUDIES

The arrival of numerical approaches to optimize forming operations dates back decades ago. Few studies on the piercing process were found in technical literature before the utilization of numerical techniques; they consist of experimental investigations carried out on a real piercing mill and mainly focused on the influence of processing parameters (i.e. rolls velocity, geometry and tilting, plug features) on the quality of the obtained hollow part and on the efficiency of the mill [50-52].
More interesting investigations on piercing process were carried out adopting finite element modeling. The first studies in this context [53, 54] focused on the analysis of material flow and distributions of strain components during deformation; the developed models were quite simplified compared to the real plant configuration in view of the low computational capabilities characteristic of those years. Although in a simplified numerical model with questionable calibration procedure, Mori et al. gave one the first example on the application of a damage criterion (in the case, Oyane damage model was used) for the prediction of the Mannesmann effect [55].

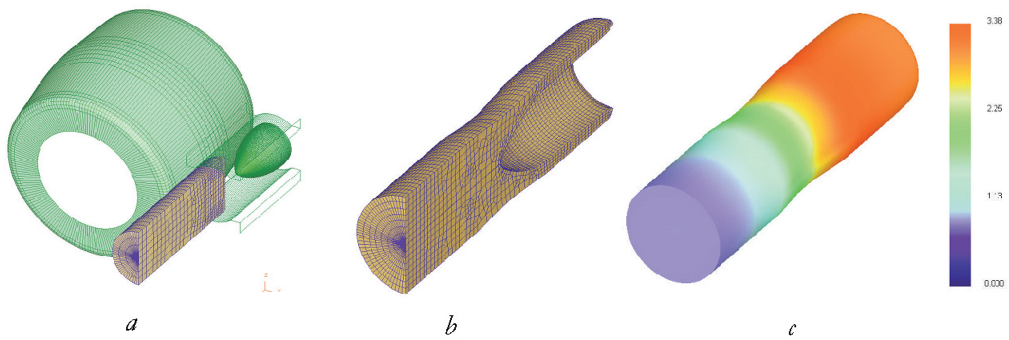

Fig. 2.17 Parts set-up (a), deformed mesh (b) and correspondent equivalent strain prediction in the ALE method based simulation [56]

Different approaches are suitable for the numerical simulation of the piercing process. Yang et al. [56] proposed a solution based on the so called ALE method (according to the Arbitrary Lagrangian Eulerian formulation) that gave excellent results in terms of material flow prediction with limited computational time if compared to the other numerical techniques. A validation of the model was made by comparing the geometry of the numerical pierced part with the same obtained in a real plant. Some details related to this study are reported on Fig. 2.17.
A particular finite element model according to the steady-state formulation was developed by Komori [57]: the effects of rolling condition modifications (rolls and plug geometry, parts positioning, kinematics) were observed on various rolling properties (forces on rolls and plug, tube characteristics, material flow). A validation of the numerical prediction was performed with an experiment using Plasticine.
It was proven that the last two works presented here [56, 57] represent suitable tools for the prediction of the hollow part geometry and the evaluation of loads on the equipment during the piercing operation. On the other hand, if the requirement is the modeling of the real process conditions and the real material behavior during the deformation, these two approaches are both limited since the Mannesmann effect was not taken into account. Fracture was not considered in general and the piercing was performed through plastic deformation.
A more accurate numerical simulation of the piercing process should consider the crack initiation due to the Mannesmann effect along the billet axis, in view of the role of this fracture on the tube quality and plug life, as explained in chapter 1.
Limited references concerning the Mannesmann effect investigation and modeling of its consequences through numerical simulation can be found in technical-scientific literature.
The characterization of the Mannesmann effect also involves the cross wedge rolling process. It is well known that a central fracture due to this phenomenon is a typical defect in components obtained through cross wedge rolling under certain working conditions [58-61]. In particular, Dong et al. [60] predicted the state of stress on a rolled bar and confirmed the presence of the secondary tensile stress component, which is typical of the Mannesmann effect and at the basis of the central crack observed when the rolled part was sectioned. A three dimensional finite element model of a complete cross wedge rolling operation was proposed and developed with the code Forge3® by Piedrahita et al. [61, 62]. Considerations related to a crankshaft central defect are found in these two works, the state of stress was analyzed and the

failure condition was discussed also with the aid of damage models implementation.

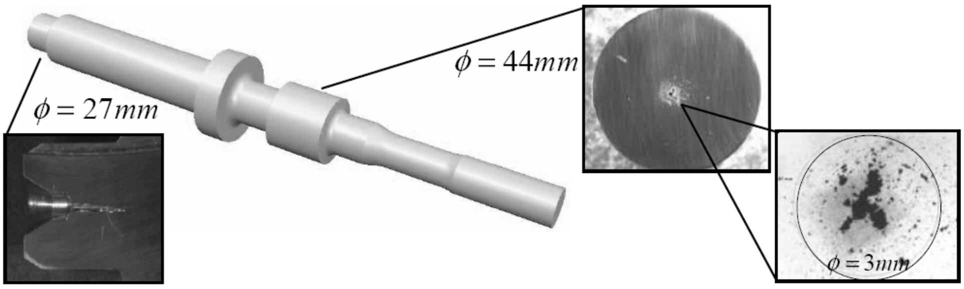

Fig. 2.18 Internal defects due to the Mannesmann effect on a cross rolled crankshaft [61]

Berazategui et al. [63] developed a very accurate tube piercing finite element model which took into consideration the Mannesmann effect . An Eulerian formulation was implemented into the code in which the mesh was fixed and the material moved inside it (Fig. 2.19).

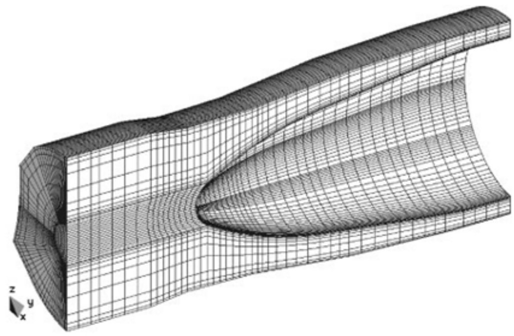

Fig. 2.19 Example of Eulerian finite element mesh for piercing simulation [63]

Simplifications were adopted in the numerical analysis of Berazategui et al.: isothermal condition (constant temperature of the billet material during the process), perfect sticking between rolls and billet and also there was no prediction of the Mannesmann fracture. In fact, the Mannesmann effect was represented by a "damaged cone" (placed just in front of the plug and whose length was determined through experimental in-plant investigations) in which the material strength is close to zero. Despite these simplifications, numerical prediction of the hollow part was in agreement with the industrial test under different rolling conditions. The model was suitable for the prediction of the material flow and represented a valid tool for the observation of rolling parameters influence on the process design; Fig. 2.20 reports an example of effective strain distribution resulted from the computation.

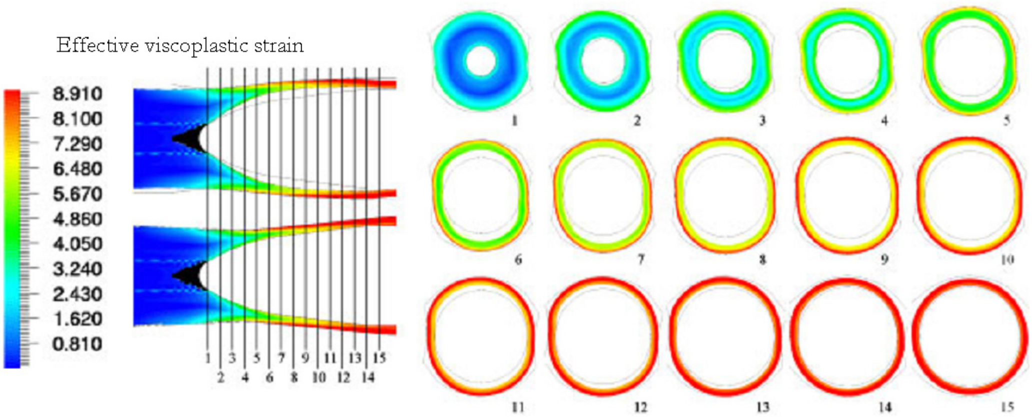

Fig. 2.20 Effective strain distribution [63]

One of the most complete studies on Mannesmann piercing was done by Ceretti et al. [64-67] using the commercial code DEFORM®. In order to model the Mannesmann effect, a two dimensional numerical simulation in isothermal conditions was developed using a schematization of the three dimensional process for building the tool profile. The main advantage of the 2D model is the significant reduction of calculation time. The authors justified this plane strain approximation with a preliminary 3D simulation that had shown the negligible value of the axial stress component with respect to the two components on the transverse section of the bar. A first validation of the developed 2D model was done by comparing material flow prediction with the fiber distribution which was observable through a macrographic analysis on a sectioned real semi-pierced round bar. Damage was modeled using the Cockcroft & Latham criterion and the critical damage value with respect to fix the central crack initiation was determined measuring the longitudinal position of the Mannesmann cone obtained with a in-process stop during industrial tube piercing (Fig. 2.21).
On the basis of the two dimensional simulation results, the authors developed a fully three dimensional model including the plug to predict the complete hollow forming operation (Fig. 2.22). Damage characterization was maintained the same as the previous but its calculation was limited to a restricted volume

across the billet axis [67]. The validation of the numerical approach was done comparing several transversal cross sections of the tube obtained numerically and industrially.

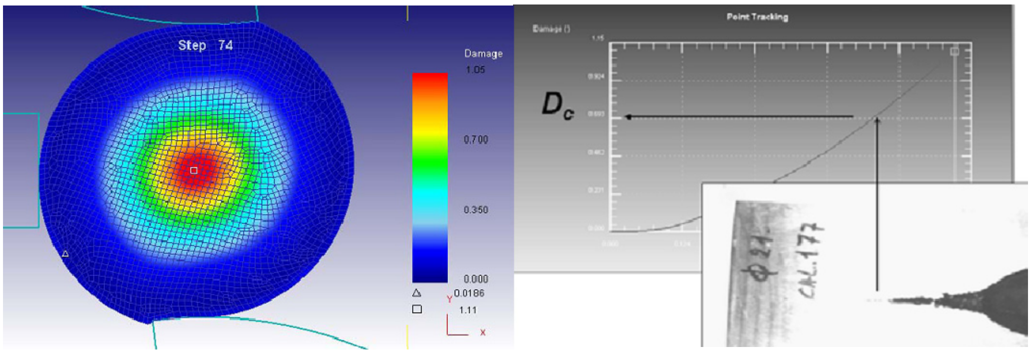

Fig. 2.21 2D finite element model of non-plug piercing [64-67]

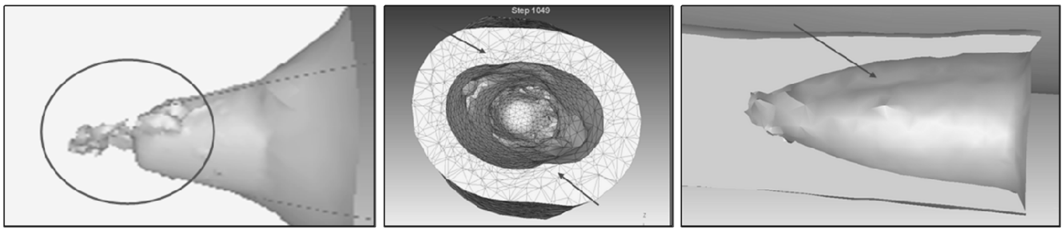

Fig. 2.22 3D finite element model of tube piercing [67]

The last application reported here regarding the numerical modelling of the Mannesmann piercing refers to recent work carried out by Pschera et al. [68] using the commercial code Forge®. The capabilities of several damage models were tested for the prediction of both Mannesmann fracture initiation and its propagation according to an uncoupled approach to fracture.

CHAPTER 3

THE APPROACH

Although the Mannesmann piercing process has been used since the 19th century, there needs to be more scientific knowledge on fracture mechanisms in order to optimize the industrial set-up and obtain higher quality products.
In spite of the great importance that fracture, due to the Mannesmann effect, has on the quality of the piercing operation, "trial and error" is still the main industrial method used to find the best working parameters in the early stage of the piecing set up. The knowledge of the crack axial position before production would grant relevant advantages from the tube manufacturer point of view:

- numerous trials could be avoided before reaching the optimal forming set up, material could be saved and plug service life could be increased;
- it is possible to improve the quality of the hollow part by optimizing the other sensitive parameters (i.e. rolls velocity or rolls axis inclination) once the general operating condition has been chosen, in relation to the

characteristics of the tube to form.

Several studies have been carried out on piercing modelling through numerical simulation. The finite element method has demonstrated to be an especially helpful and inexpensive tool for the engineering phase of manufacturing. In previous chapters some examples have been reported„ mainly regarding damage model implementation into an appropriately defined numerical model of the process.

The objective of this work is to model the fracture due to the Mannesmann effect during the piecing process, paying special attention to the particular material properties, often neglected, but fundamental for the fracture behaviour. In fact, there are no damage models in scientific literature that are capable of describing the Mannesmann fracture initiation and that take into account at the same time the workability characteristics of continuous cast billets.

A scheme summarizing the combined numerical-experimental techniques adopted in this research is reported in Fig. 3.1:

- Industrial trials; the representative case that the investigation has been based on is the piercing operation on the real plant mill. The tests have been carried out without the plug since the Mannesmann effect is related to a secondary tensile stress component only due to the rolls action on the billet.
- Finite element modelling; numerical analysis of a non-plug piercing process that has been used to investigate the stress and strain states through which Mannesmann fracture can arise.
- Material testing to investigate the workability of the tube steel under the working condition of the industrial process. The rheology and the effect of material properties on the fracture behaviour have been studied using laboratory tests.
- Micro-structural analysis to characterize the continuously cast billet in terms of phase distribution and porosity amount using metallographic techniques.
- Damage analytical modelling and inverse analysis techniques; after a sensitivity study regarding different damage models capabilities, Continuum Damage Mechanics resulted the most suitable damage approach for the Mannesmann fracture prediction and it was accurately calibrated using hot tensile test and inverse analysis technique. In order to take into account the typical properties of a continuously cast billet and consider their effect on the damage modelling, a modification was introduced into Lemaitre 's standard model.

Once the above mentioned techniques have been applied, the calibrated numerical model of non-plug piercing was validated by comparing the main features of the Mannesmann fractures respectively obtained in the real plant and in the numerical simulation and the feasibility of the proposed approach was evaluated.

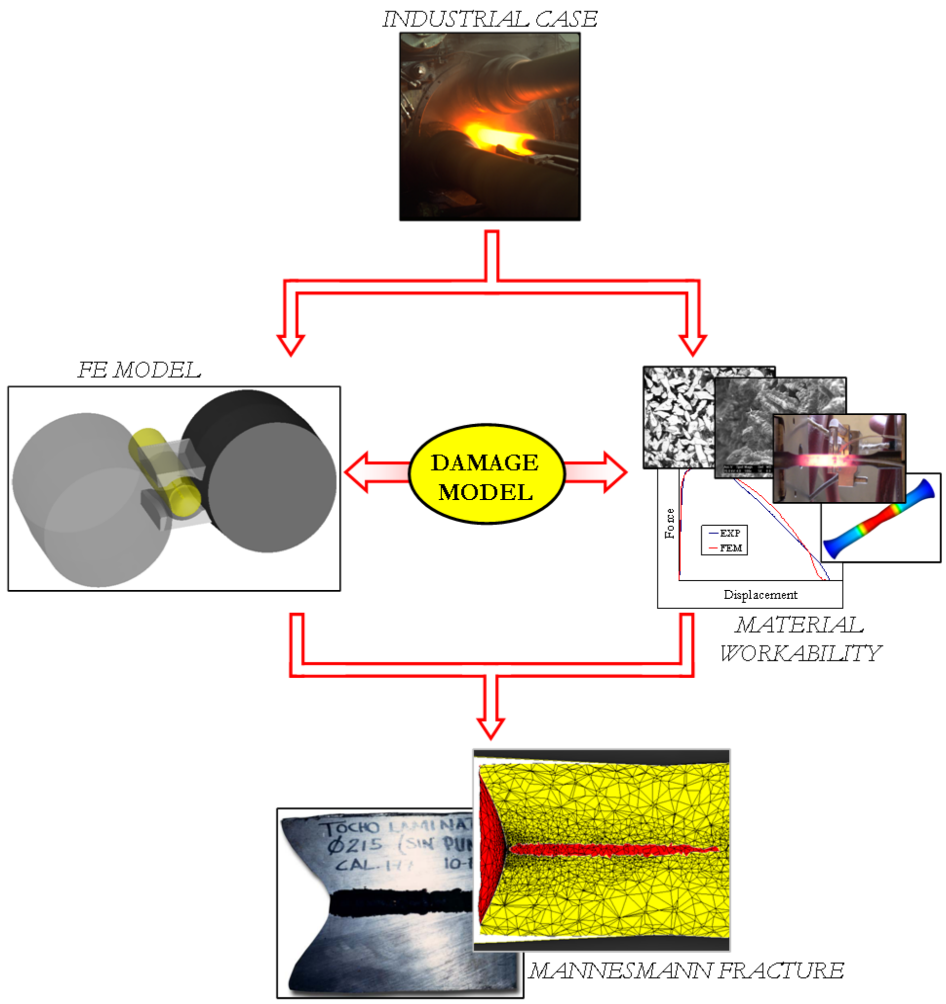

Fig. 3.1 The work approach

Initial material properties such as void content and phase distribution are usually neglected on the numerical modelling of forming processes: this work reports the integration of these micro-structural aspects with rheological and workability properties of the tube steel under process conditions. The calibrated damage model is the tool used for the implementation of all these material characteristics on the numerical simulation in order to obtain the most accurate prediction of the Mannesmann fracture.

CHAPTER 4

EXPERIMENTS

4.1 INTRODUCTION

The investigation about the process conditions leading to the Mannesmann effect started from the realization of the Mannesmann fracture in the real piercing mill. These industrial tests are the basis on which the numerical model is developed and they are also the necessary data for its final validation.
An accurate modeling of the Mannesmann effect then needs an in-depth laboratory characterization of the material properties under the real metalworking condition. A continuously cast billet of the steel tube coming from the same batch of the industrial trials was examined focusing on the aspects related to rheology, workability and micro-structure.
Experimental studies carried out in the plant and laboratory have provided

the necessary information for the work to continue.

4.2 MANNESMANN NON-PLUG PIERCING TRIALS

Different tests on the industrial piercing mill were carried out in order to obtain the typical fracture along the axis of the billet due to the Mannesmann effect. Since the pure Mannesmann effect is due uniquely to the rolls action, the plug was removed from the traditional set up. The cylindrical billet obtained through continuous casting, after a pre-heating in the furnace, was introduced on the mill; the rolling operation was stopped only when more or less half of the billet length was deformed.
By this way, a semi-rolled cylindrical part was obtained and sectioned longitudinally and the length of the Mannesmann fracture was measured with respect to the minimum roll gap.
Different testing conditions, as reported in Tab. 4.1, were chosen varying the velocity of the rolls or the minimum rolls gap (usually named “draft”) and their effect on the length of the Mannesmann facture was observed.

Billet diameter	200 mm		
Feed angle	xx		
Entering billet temperature	1250°C		
	Engine velocity [rpm]	Draft [mm]	Mannesmann cone length [mm]
Test 1	xxx	xxx	112
Test 2	xxx	xxx	100
Test 3	xxx	xxx	105

Tab. 4.1 Industrial trials condition

The pictures of the three different Mannesmann cones obtained rolling the billet without the plug are reported in Fig. 4.1. The white straight line drawn on each sample in Fig. 4.1 represents the minimum rolls gap, from which the Mannesmann cone is measured.
Starting from this first experimental evidence of the Mannesmann effect, material properties have been investigated and the numerical model has been implemented.

Test 1	Test 2	Test 3
	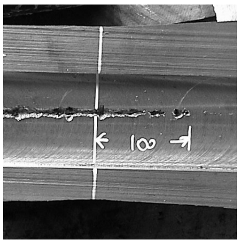	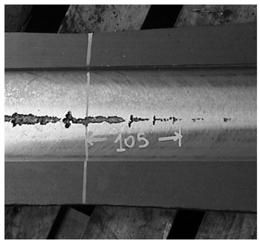

Fig. 4.1 Mannesmann cone lengths from industrial non-plug trials

In order to investigate the rupture mechanism related to the axial crack formation due to the Mannesmann effect, a portion of the crack obtained from trial n. 2 was extracted and examined using a scanning electron microscope (SEM).

Different morphological aspects were found on the fracture surface:

- large regions characterized by an undeformed dendritic structure (Fig. 4.2) in which numerous inter-granular fractures were observed Fig. 4.3);

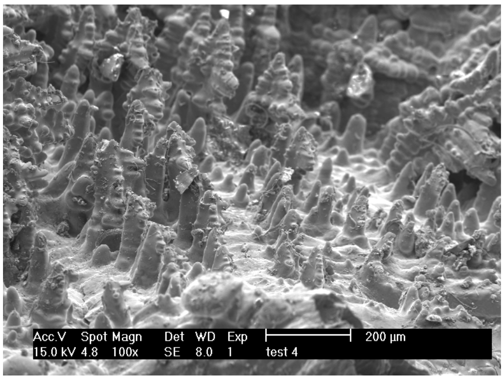

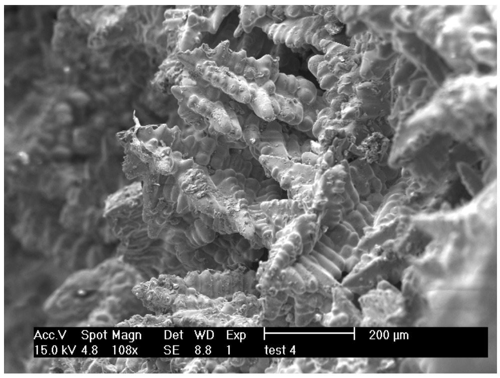

Fig. 4.2 Undeformed dendritic structure on a Mannesmann fracture surface (Magnitude 100x)

- limited extended zones on which plastic deformation happened and fracture occurred in ductile mode (Fig.4.4).

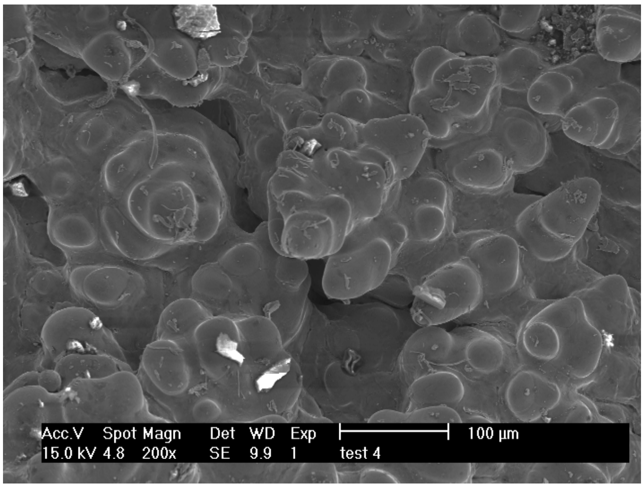

Fig. 4.3 Example of inter-granular fracture on the dendritic structure (Magnification 200x)

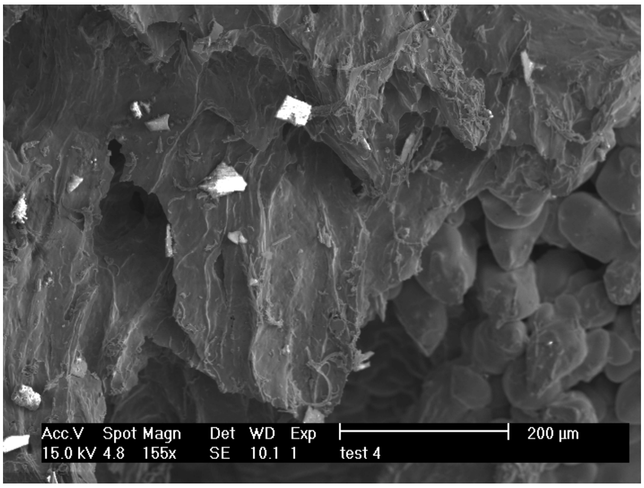

Fig. 4.4 Mannesmann fracture surface with ductile properties (Magnitude 150x)

Globally, the SEM analysis of the Mannesmann fracture surface showed it cannot be considered a pure ductile one, in fact limited regions were subjected to evident plastic deformation. Wide areas with undeformed dentritic structure characterized by inter-granular fractures were observed and can be traced to a low strain rate fracture condition, typical of decohesive fracture modes.

4.3 CONTINUOUS CAST MATERIAL PROPERTIES

During industrial tests to obtain the Mannesmann fracture, a portion of the cylindrical billet from the same batch used for the trials was set aside in order to study the steel behavior with laboratory experiments.
A typical manganese low alloyed steel for seamless tube manufacturing (xxx according to EN 10297-1) was used and its composition is reported in Tab. 4.2.

C	xxx
Mn	xxx
Si	xxx
P	xxx
S	xxx
Ni	xxx
Cr	xxx
Mo	xxx
Cu	xxx
Sn	xxx
Al	xxx
V	xxx
Nb	xxx
Ti	xxx
W	xxx

Tab. 4.2 Chemical composition of xxx steel used for the work (weight %)

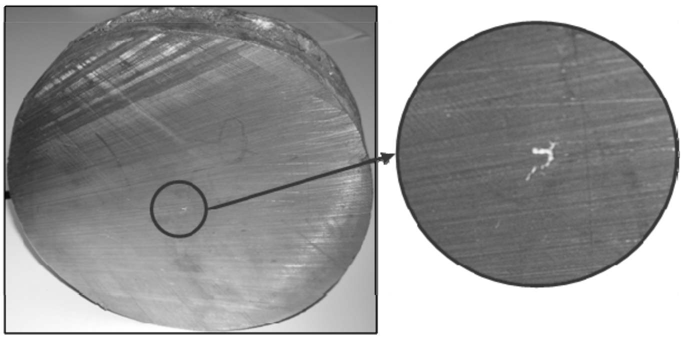

Fig. 4.5 Diametral section of the billet with evidence of a void due to shrinkage on the central region

The original cylindrical billet (200 mm diameter) was obtained through continuous casting. The importance of taking into account the consequences on material properties due to the solidification and cooling phases characterizing this particular manufacturing process will be demonstrated. In fact, simply a diametrical section of the billet could cause the central void due to shrinkage visible to the naked eye (Fig. 4.5).

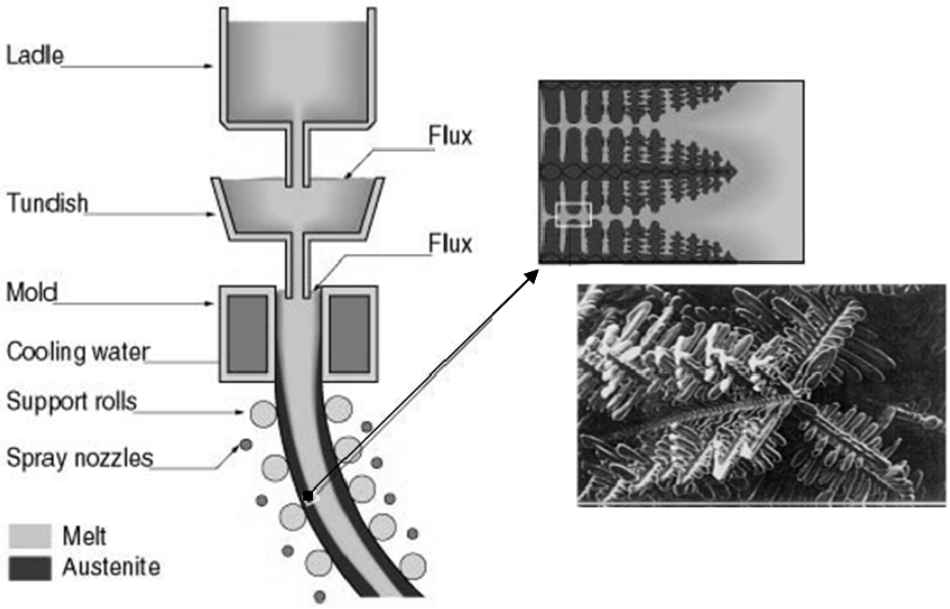

Fig. 4.6 Solidification in continuous casting process

As schematized in Fig. 4.6, the solidification of the melted steel starts at the outer surface of the cylinder thanks to contact with the mould: the typical dendritic structure grows towards the billet centre that is the last solidifying portion.
An example of the grain distribution obtained on a square section billet after the solidification is reported in Fig. 4.7. The instantaneous cooling of the outer surface provokes a fine equiaxed texture, then the dendritic growth causes the columnar microstructure in view of the high temperature gradient, while coarse equiaxed grains are present in the central zone of the billet due to the lower cooling rate.

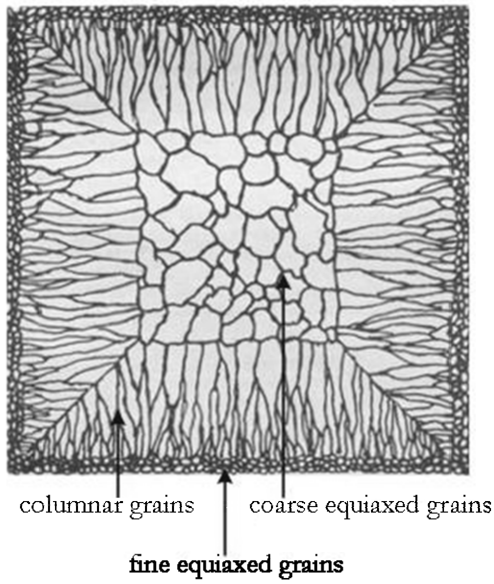

Fig. 4.7 Grain distribution on a continuously cast squared section billet

During the following laboratory experiments, in view of the various grain properties on the billet, it is fair to wait for different workability responses of the material in relation to its radial location on the billet section. This aspect is taken into account for the experiments set up in terms of sample location on the cylindrical billet, in particular samples extracted along the billet axis were distinguished from the transversal ones and their distance from the centre was considered.
The rheological properties of the tube steel have been investigated by means of hot compression test under piecing working conditions while the workability of the material has been studied using hot tensile test.

4.3.1 Rheological characterization

The hot compression test has been chosen as the proper way to determine the rheology of steel in terms of flow curves that are then necessary for the correct material implementation on the numerical model. This choice can be justified by two main aspects:

- compression test is closer to the compressive state of the billet that globally characterizes its rolling during the piercing operation;
- compression test with minimum friction is less affected by instabilities

and damage phenomena than a tensile test.
With the objective of characterizing the material behaviour under process condition, testing parameters have been chosen according to previous investigations carried out by the industry in order to determine the working window in terms of temperature and strain rate evolution in the billet material during the piercing operation [69].
Tab. 4.3 summarizes the testing parameters and the sample geometry used for the hot compression test campaign.

Temperature [°C]	1050 ÷ 1250	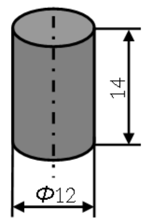
Strain	0 ÷ 0.8	
Strain rate [s^{-1}]	0.05 ÷ 20	
Samples extracted from the central and the peripheral region of the initial billet		

Tab. 4.3 Hot compression test conditions and specimen geometry

All the compression tests have been carried out on the thermo-mechanical simulator Gleeble 3800™ (Fig. 4.8) set up in the compression mode.

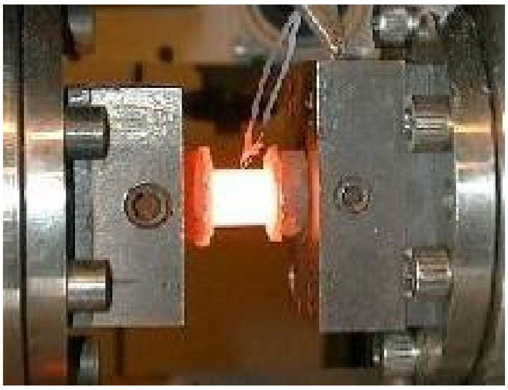

Fig. 4.8 Gleeble 3800™ system in compression configuration

In order to minimize the effect of friction and avoid the thermal gradient on the flat surfaces of the specimen, an appropriate interface has been interposed between punches and specimen. A combination of two alternate foils of graphite and tantalum, acting respectively as lubricant and thermal barrier, has been applied (Fig. 4.9). Moreover, the flat surfaces of the specimen are coated with molybdenum disulfide to avoid welding the specimen to the dies during hot deformation experiments.

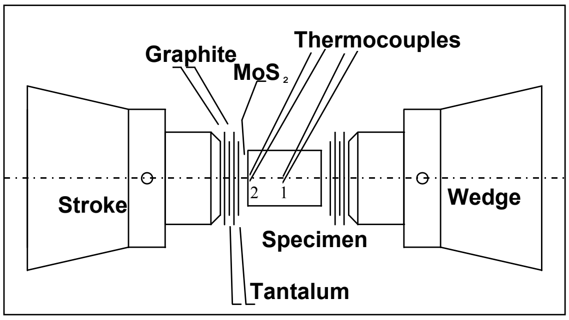

Fig. 4.9 Scheme of the compression test set up

CONFIDENTIAL

Fig. 4.10 Flow curves obtained through hot compression test

An example of material flow curves for different temperature and strain rate conditions are reported in Fig. 4.10. The negligible influence on the rheological behaviour of the samples direction extraction is evident with respect to the billet axis orientation.
A non-linear regression technique has been used for the experimental data fitting in order to identify the rheological law parameters for the material rheology implementation into the numerical model. In particular, a reduced formulation of the Hansel-Spittel law has been chosen to represent the flow stress dependency on strain, strain rate and temperature (eq. IV.1).

$$\sigma = A e^{T m_1} \varepsilon^{m_2} \dot{\varepsilon}^{m_3} e^{\left(\frac{m_4}{\varepsilon}\right)} \qquad \text{(IV.1)}$$

A	m_1	m_2	m_3	m_4
xxx	xxx	xxx	xxx	xxx

Tab. 4.4 Rheological law coefficient

The reduced form in place of the original Hansel-Spittel one has been adopted in order to shorten the computation time having previously evaluated its accuracy on material behaviour description.

CONFIDENTIAL

Fig. 4.11 Example of the Hansel-Spittel model application (eq. IV.1)

4.3.2 Workability investigation

A workability investigation has been carried out in this work in order to model the material response when subjected to the thermal-mechanical conditions typical of the Mannesmann effect.
As Mannesmann fracture appears due to a secondary tensile stress component in the centre of the billet during the first stage of piercing operation, the uniaxial hot tensile test has been chosen for the experimental study. Experimental tests were carried out on a Gleeble 3800™ machine in the tensile set up and equipped with a diametral extensometer to monitor the instantaneous section of the sample after necking (in order to obtain the instantaneous strain value).
Tensile testing conditions have been fixed according to the industrial non-plug piercing trials and to some preliminary numerical results about the strain field during the deformation of the billet [70]. In the following chapters, the correctness of these first assumptions will be amply demonstrated thanks to the developed numerical model results.
Tensile specimen geometry according to ASTM guidelines (ASTM E8-96a, Standard Test Methods for Tension Testing of Metallic Materials; ASTM E21-92, Standard Test Methods for Elevated Temperatures Tension Test of Metallic Materials) is reported in Fig. 4.12 while Fig. 4.13 refers to the tensile configuration of the Gleeble 3800™ simulator.

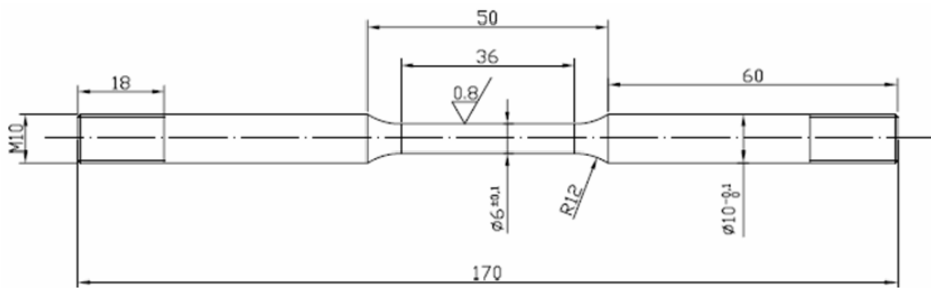

Fig. 4.12 Hot tensile test sample geometry

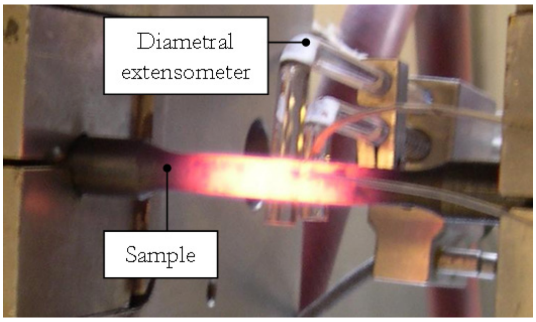

Fig. 4.13 Gleeble 3800™ system in tensile configuration

Tab. 4.5 summarizes the conditions adopted for the hot tensile test campaign.

Temperature	1250 °C
Strain rate	$5 \cdot 10^{-4} \div 0.5\ s^{-1}$
Location on the billet section	Centre and Periphery
Tilting with respect to the billet axis	Normal and Parallel

Tab. 4.5 Hot tensile test experimental conditions

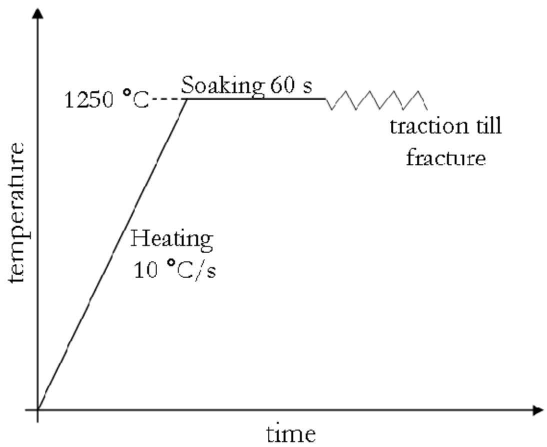

Fig. 4.14 Thermal cycle for the hot tensile test

Each test performed was characterized by the thermo-mechanical cycle reported in Fig. 4.14:

- heating phase, in which the sample central region was heated up from

room temperature condition to the testing temperature of 1250 °C maintaining a constant heating rate equals to 10 °C/s;
- soaking period equals to 60 s performed with the aim to homogenise the thermal condition on the material;
- isothermal tensile deformation till fracture under constant strain rate conditions, measuring the current values of force, displacement and sample diameter.

The sample extraction procedure from the cylindrical continuously cast billet was very accurate: samples were distinguished with respect to their inclination (parallel or normal to the billet axis) and to their radial position on the billet section (Fig. 4.15a-b).

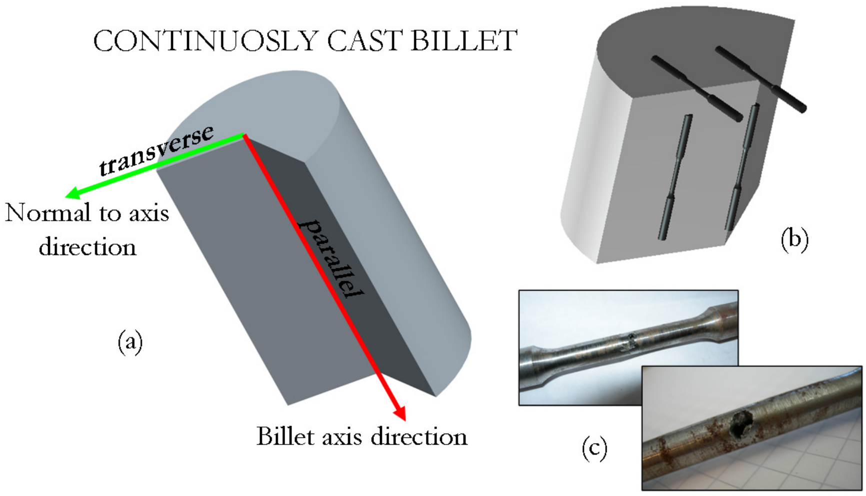

Fig 4.15 Schematization of samples extraction

Fig. 4.15c reports an example of initial defect due to shrinkage during the steel solidification on a typical sample extracted from the billet centre. This evident porosity is a clear first demonstration of the importance of distinguishing the radial location of the tested material.

Each experimental condition was repeated at least 5 times, however, the random voids distribution even in specimens machined from the same position in the cast billet can assure repeatability of results (in terms of stress and strain at fracture) only in the range of ±20%.

CONFIDENTIAL

Fig. 4.16 Effect of the sample tilting with respect to the billet axis on material behaviour at different strain rates

CONFIDENTIAL

Fig. 4.17 Difference on material strength due to the radial location on the billet

Observing Fig. 4.16 related to tests on peripheral samples, it can be said:

- the investigated material has evident sensitivity to the strain rate;

- samples extracted parallel to the billet axis show in general lower values of flow stress but higher strain at fracture than the normal ones;
- fracture strain increases if strain rate increases and this behaviour can be related to different fracture mechanisms.

Evident differences on the material resistance to deformation are related to the radial position in the billet section on which samples are extracted. Central material is characterized by lower strain at fracture and lower maximum stress than the one extracted from the billet peripheral annulus (Fig. 4.17).

These differences on the material behaviour are due to the properties distribution in each specimen induced by casting; for example porosities and voids due to the cooling phase are larger and more numerous in the centre of the billet, and additionally they are characterized by a stretched shape in the casting direction (that corresponds to the rolling direction during piercing).

In view of the results obtained on this experimental tensile test campaign, referring to a 200 mm diameter cylindrical billet, "centre" refers to a billet zone of an approximately 60 mm diameter, where the dependence of mechanical behaviour from a radial position was found to be evident. The "periphery" refers to the billet zone from a 60 mm to 200 mm diameter, where the material tensile response was proven to be less dependent on the distance from the billet centre.

Finally, the fracture surfaces obtained on the tensile specimens were observed using scanning electron microscopy.

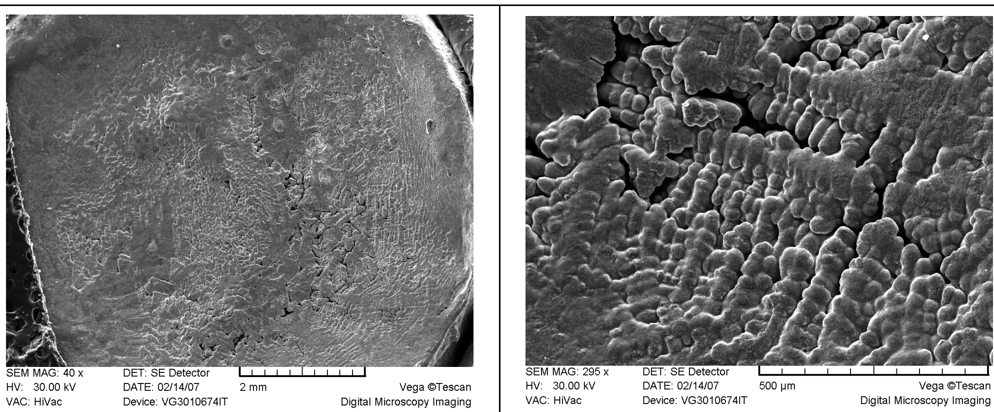

(a) Magnification 40x | (b) Magnification 300x

Fig. 4.18 Fracture surface on a central tensile specimen tested at the lower strain rate condition ($5x10^{-4}$ s^{-1})

In particular, the strain rate conditions chosen for the experiments were representative of the different fracture modes combination that was observed with the analysis on the industrial trials fracture surfaces:

- the specimen tested under the higher strain rate conditions presented a pure ductile fracture accompanied by elevated plastic deformation;
- the lower strain rate test conditions provoked a fracture surface (Fig. 4.18) similar to the inter-granular one that was predominant under the typical Mannesmann effect working condition (Fig. 4.3).

4.3.3 Micro-structural characterization

In view of the experimental study on material workability, micro-structural investigations were carried out in order to find out and quantify the main causes of these evident differences on material strength as a function of the sample extraction location.

Two aspects related to the material micro-structure deriving from the solidification pattern after casting have been studied using metallographic techniques and optical microscopy:

- voids distribution inside the billet as an effect of the strong shrinkage during solidification;
- steel phase distribution in billet radial direction due to the cooling gradient.

Several samples were extracted from the cast billet section at varying distances from the centre: after the appropriate surface polishing, the voids content was determined for each sample through the digitalization of high contrast images, averaging at least ten measures of voids area fraction on the same sample.

The material extracted from the billet central zone is characterized by the highest porosity in view of the severe shrinkage due to the cooling after casting (Fig. 4.19, in which R is the billet radius 100 mm and r the radial distance of the sample).

To investigate steel phase distribution, a standard Nital 3 chemical etching was used after polishing the analysed surface. Fig. 4.20 reports the ferritic phase content with respect to the radial position from which each sample was extracted.

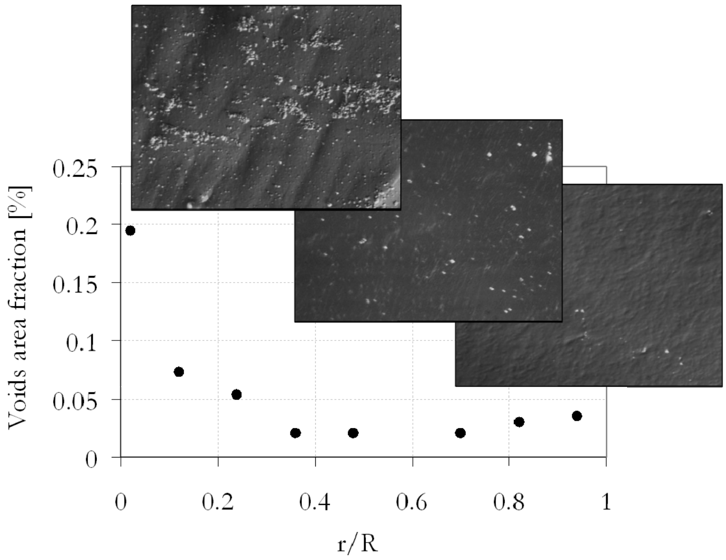

Fig. 4.19 Voids distribution on the billet radial direction

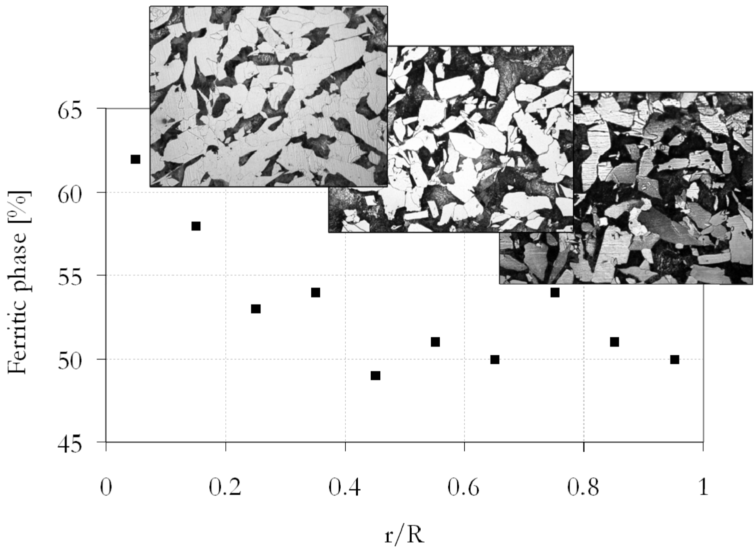

Fig. 4.20 Radial ferritic phase content distribution on the billet

In view of the analysis results, the billet can be divided into two portions:

- the *centre* that is represented by an inner cylinder of approximately 60 mm in diameter in which there is an evident gradient of ferritic phase and voids content from the billet axis;

- the *periphery* that is represented by the outer annulus of the billet in which ferritic phase content and porosity are low and can be considered constant.

A fundamental remark can be made after the analysis: lower strength of the central material shown in tensile test can be justified effectively by both higher voids and ferritic phase content, this conclusion should be taken into account during the modelling of the fracture behaviour of the tube steel.

4.4 CONCLUSION

The experimental campaign carried out on the steel tube under industrial working conditions made it possible to characterize its rheological behaviour, evaluate its workability and describe the radial distributions of voids and ferritic phase in a cylindrical continuously cast billet.
The particular distribution of the properties characterizing the initial billet was investigated: the importance of distinguishing the material in relation to its radial location on the billet section was demonstrated.
These activities made it possible to obtain the necessary material parameters for the development of an accurate numerical model.

CHAPTER 5

FINITE ELEMENT MODELLING OF THE MANNESMANN EFFECT

5.1 INTRODUCTION

The main objective of the numerical simulation was to reproduce the critical working condition of the industrial piercing process in which the cavity due to the Mannesmann effect initiates. A finite element model of the non-plug piercing operation was developed in order to predict the stress/strain state typical for the fracture arising.
The typical thermal-mechanical condition leading to the Mannesmann effect was reproduced numerically thanks to the implementation of the necessary material parameters previously determined through experimental testing.
Once the numerical model was developed and properly calibrated, it was

possible to evaluate the critical material state leading to Mannesmann fracture and use damage modeling for its characterization.

5.2 DEVELOPMENT OF THE NON-PLUG PIERCING NUMERICAL MODEL

Rolling condition realized during industrial trials was reproduced numerically using the commercial finite element code Forge®.

5.2.1 Geometrical and kinematical settings

The tools and billet geometrical features and the kinematical parameters were introduced into the numerical model according to the condition of trial n. 2 (refer to Tab. 4.1). In Fig. 5.1, the set up implemented into the code: the two skew conical rolls rotate in the same direction and two guides (usually named "shoes") were positioned in order to guarantee the billet alignment during rolling. Rolls and guides were modeled as rigid bodies while an elastic-viscoplastic behavior was assigned to the billet according to the Hansel-Spittel rheological law previously calibrated through the compression test campaign on the tube steel.

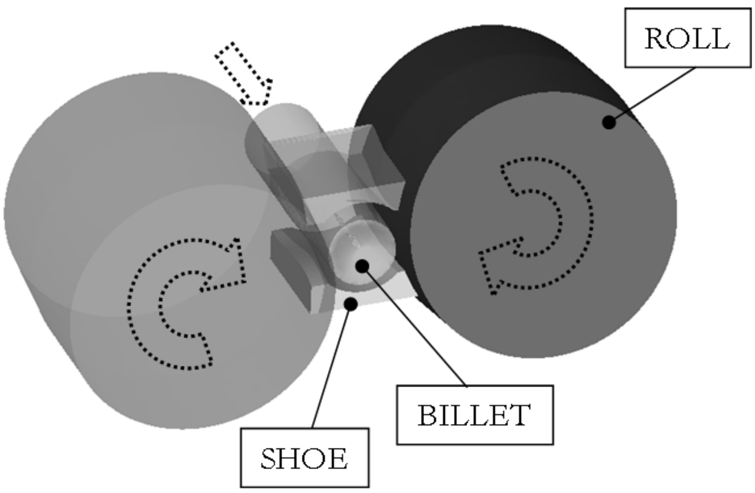

Fig. 5.1 Finite element model layout

5.2.2 Boundary conditions

Friction at the billet-rolls interface is a critical parameter in controlling the billet advancement during the process.
The proper value of friction factor was fixed equal to 0.8 according to Tresca law (Tab 5.1) following technical guidelines for typical hot forming numerical modeling [75] in order to avoid excessive sliding (efficiency higher than 90% with respect to the theoretical condition of pure rolling).

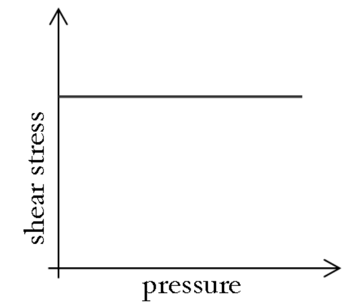	$\tau = m\frac{\sigma_0}{\sqrt{3}} = mK(T,\dot{\varepsilon}) = mA$ *m=0.8* - friction factor σ_0 - yield stress K - consistency A - Hansel Spittel consistency

Tab. 5.1 Tresca friction law

Initial billet temperature was set equal to 1250 °C according to the industrial trials condition.
Unlike the case of friction, the heat transfer at the billet-rolls and guides-rolls interfaces is not a critical parameter for the fracture appearance in relation to the process speed and the thermal inertia of the billet. This is confirmed by a sensitivity analysis carried out on typical industrial process conditions; accordingly typical hot forming heat transfer data are assumed [75]: heat transfer coefficients for the billet were set with the air and with the tools (which temperature was set equal to 50 °C, according to industrial suggestions) according to Tab. 5.2.

interface	***heat transfer coefficient [W/m²K]***
billet - tools	10^4
billet - air	10

Tab. 5.2 Heat transfer properties of the billet

5.2.3 Numerical parameters

In view of the complexity of the process in terms of its numerical implementation, the simulation required some particular tricks for the time discretization [72] in order to optimize it:

- the second order Runge Kutta scheme was adopted in place of the classical Euler scheme due to its better representation capability when numerical points are subjected to large rotation. A comparison of the two approaches over a time step is given in Fig 5.2 (X_t represents the position at time t, v is the velocity and dt is the time step);
- maximum time step in the simulation was fixed equal to 0.0005 s in order to avoid excessive artificial volume increase and incorrect contact between the billet and the tools.

The numerical choices are cause of a relevant computation time increase but have made it possible to model the rolling contact conditions very accurately.

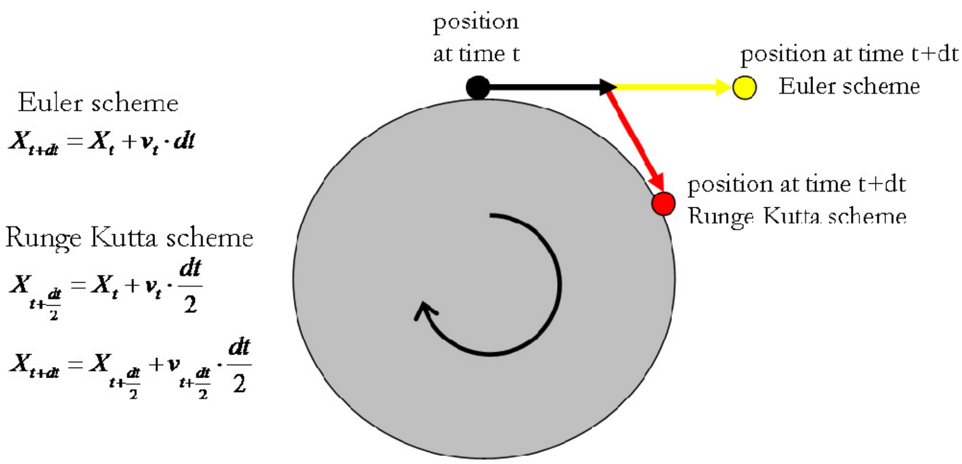

Fig. 5.2 Approaches on the numerical update over a time step

- The discretization of the billet volume is a sensitive phase during the simulation set up because of its influence on many aspects:
- fine mesh is necessary in the outer billet region in order to correctly model the contact between rolls and cylindrical billet and to guarantee reliable deformation in the contact region;
- Mannesmann effect modelling and fracture prediction require very fine mesh along the billet axis region.

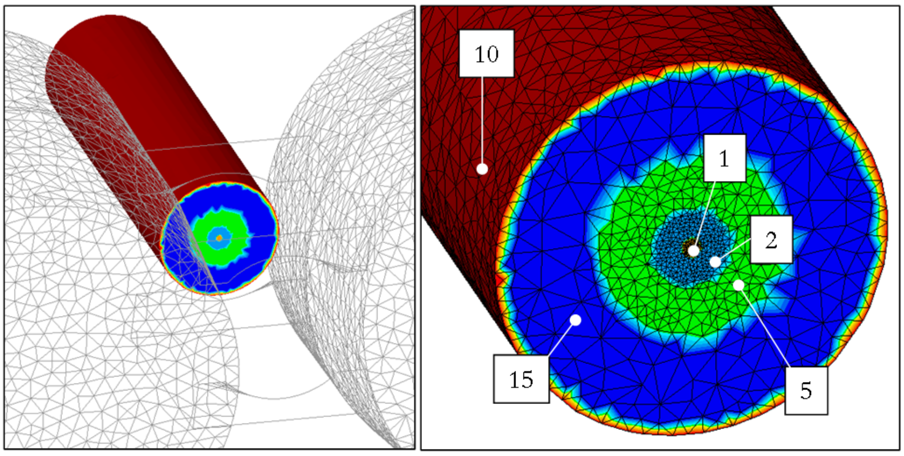

Fig. 5.3 Initial mesh distribution

At the beginning of the simulation, default mesh size was fixed equal to 15 mm, for the billet outer region the average element size was 10 mm and along the billet axis three concentric cylindrical mesh boxes were chosen in order to have a 1 mm average element size in the centre region.
Despite the considerable billet deformation during the non-piercing rolling operation, no remeshing was set and this issue will be discussed later on.

5.3 NUMERICAL RESULTS

The first objective of the non-plug piercing numerical simulation was to replicate the critical conditions leading to the Mannesmann fracture. First stress and strain states were analysed in order to verify the main assumptions adopted for the experimental campaign (i.e. loads on the material, deformation mode, strain and strain rate fields), then the capability of different damage approaches to localize the real fracture site was tested.

5.3.1 State of stress

The critical state of stress at the basis of the Mannesmann effect was thoroughly analysed thanks to internal lagrangian sensors and different cutting planes on the billet (Fig. 5.4).

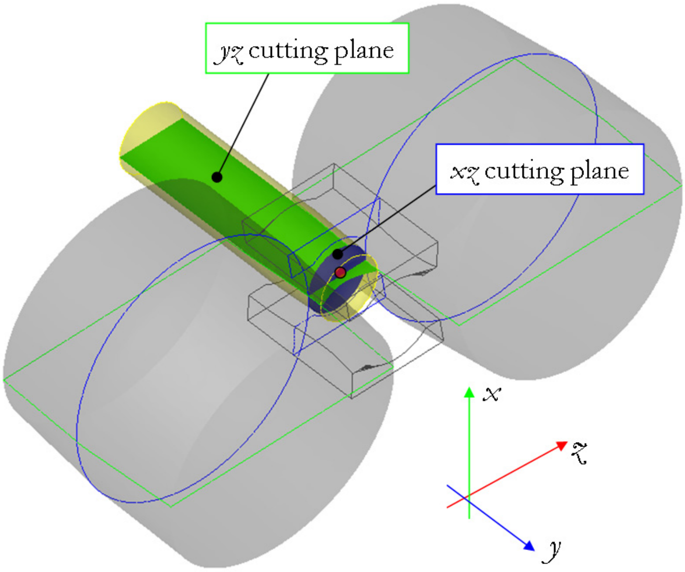

Fig. 5.4 Cutting planes and lagrangian sensor on the numerical model

A lagrangian sensor was placed on the billet axis a few millimetres from the top surface and it made it possible to follow the loading evolution on the region where the fracture was expected (red dot in Fig. 5.5).

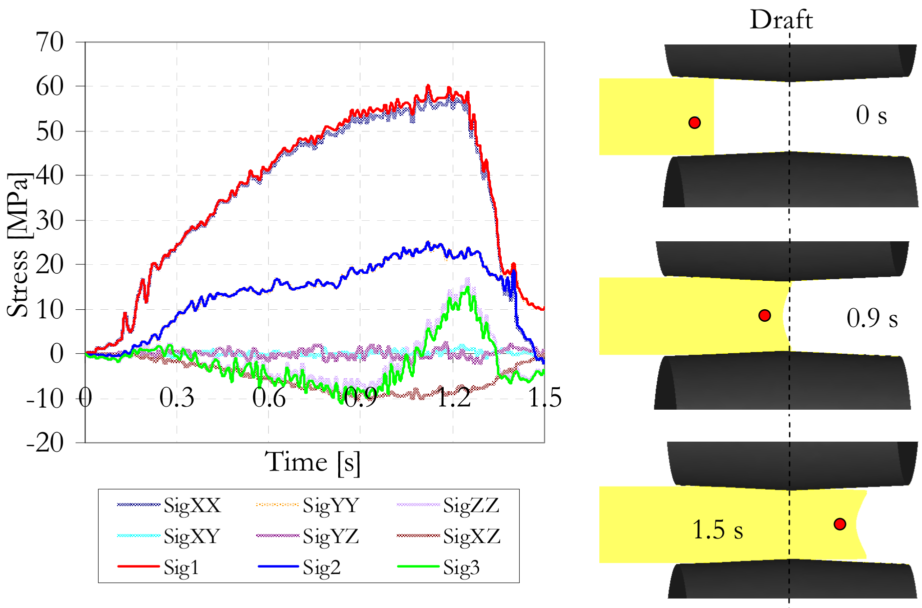

Fig. 5.5 Stress components measured by the lagrangian sensor

Referring to the stress history described by this lagrangian sensor (Fig. 5.5), some observations can be made:

- the principal stress components are oriented along the three Cartesian axis *xyz* of Fig. 5.4;
- the effect of the three shear stress components is negligible with respect to the normal ones;
- the second stress principal component, oriented along the *y* axis, is not negligible in the region where fracture initiation is expected;
- the stress components leading to Mannesmann fracture are clearly identified and their decrease is evident when the sensor leaves the rolls contact region.

The following pictures report the stress state in the billet using the *yz* and *xz* cutting planes as schematized in Fig. 5.4. They refer to a process increment where the billet is close to the minimum rolls gap (this very critical condition for fracture initiation will be shown later on).

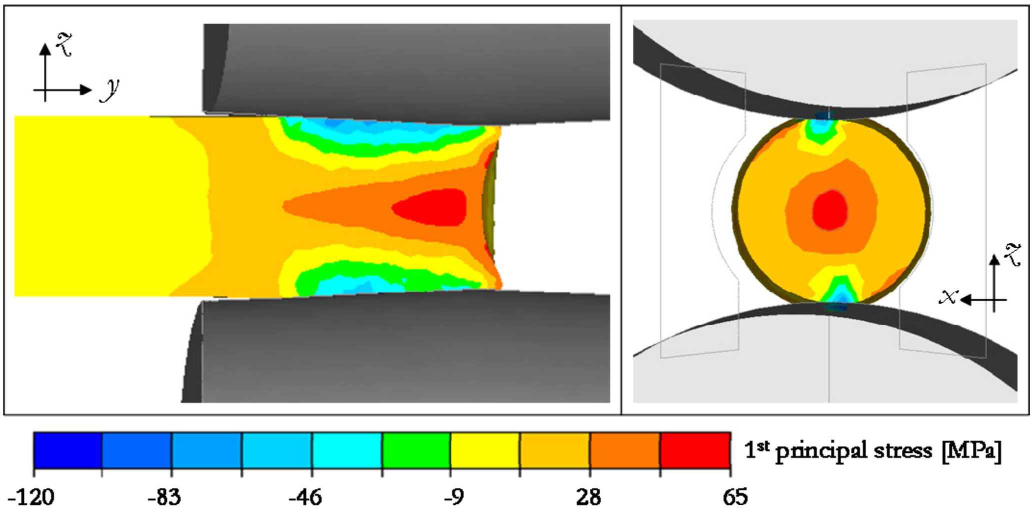

Fig. 5.6 First principal component of stress tensor

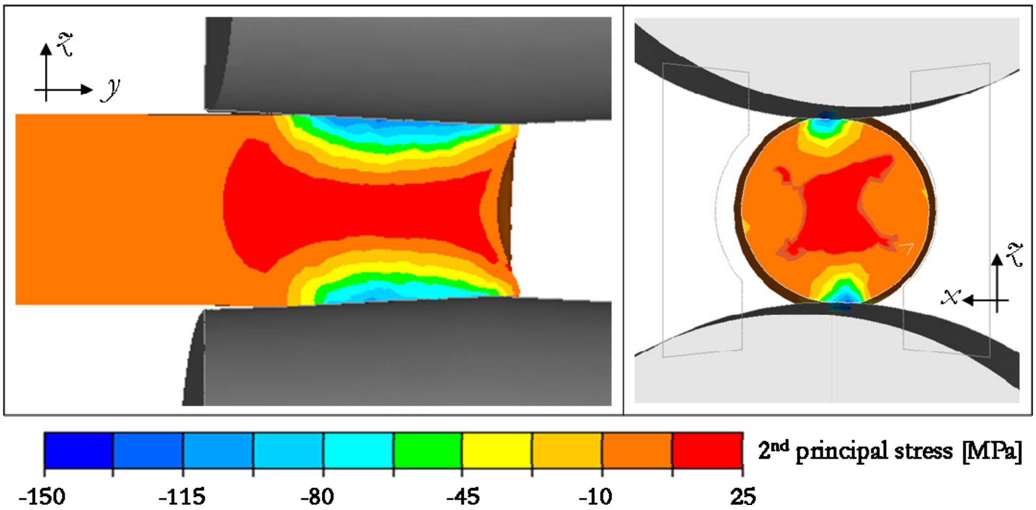

Fig. 5.7 Second principal component of stress tensor

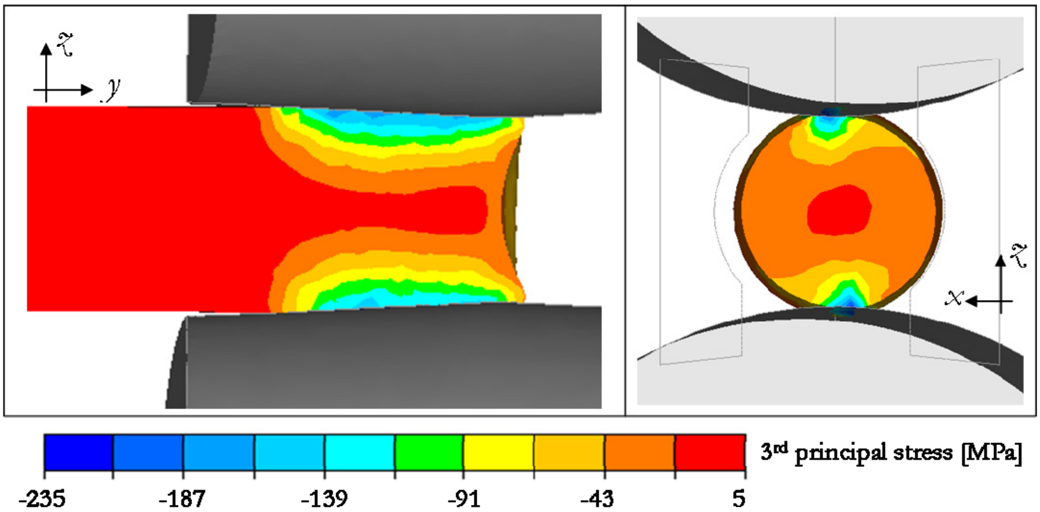

Fig. 5.8 Third principal component of stress tensor

Observing the stress state on the minimum rolls gap region, in Fig. 5.6-5.8, the three principal components are in general positive near the billet axis. The concentration of the higher first stress component value (secondary tensile stress of about 60 MPa) in the crack initiation region should play a decisive role on the establishment of the fracture critical condition in particular.
The second principal stress component in the billet central region, oriented along the *y* axis, remains positive during the rolling reaching maximum values

of about 20 MPa. It surely contributes to the critical condition for fracture initiation and can not be neglected in the modelling.
A further confirmation that the state of stress close to the minimum rolls gap can be critical for fracture initiation is given by the hydrostatic pressure distribution. In fact, Fig. 5.9 reports a localization of negative hydrostatic pressure in the expected cracking region that can be translated as a globally tri-axial state of traction.

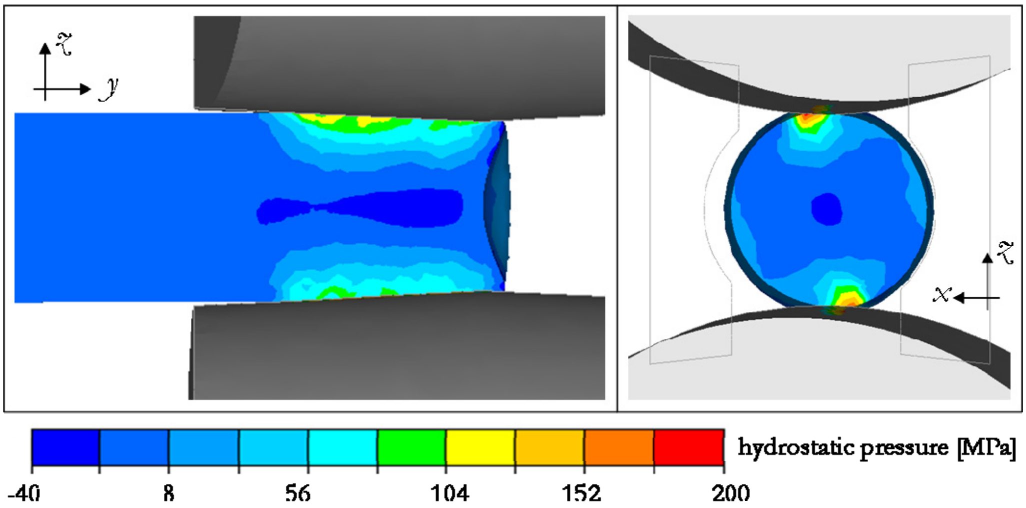

Fig. 5.9 Hydrostatic pressure distribution

The stress triaxiality field shown in Fig. 5.10 confirms again the suitable condition for fracture on the axis.

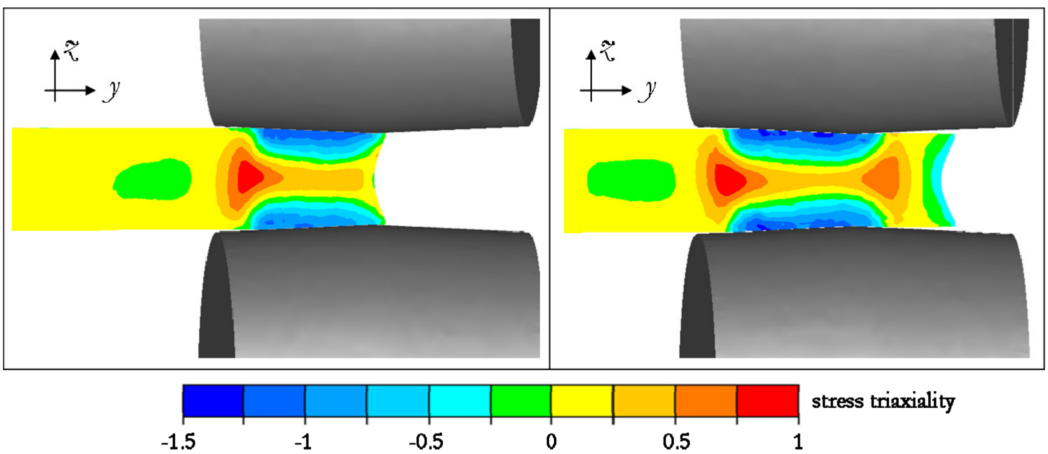

Fig. 5.10 Stress triaxiality distribution (at minimum rolls gap and at the end)

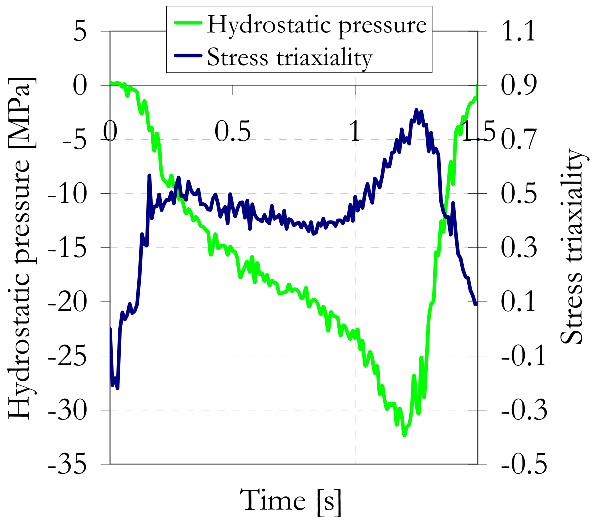

Fig. 5.11 Triaxiality and hydrostatic pressure evolution

- Considering the above reported numerical results on stress state, the hot tensile test utilized for material workability investigation can be considered the proper choice, as:
- taking into account Fig. 5.5-5.9, the first principal stress component on the expected fracture region, oriented along the x axis, can be compared to the maximum tensile stress obtained testing in tension the central material at an average strain rate of 0.5 s^{-1} on the Gleeble® machine (Fig. 4.12) and in general the state of stress can cause the material limit;
- the amount of stress triaxiality computed on the numerical model was taken between 0.5 (at the beginning) and 0.4 (close to the cracking) that is comparable with the ideal value of 0.33 characterizing a mono-axial tensile test (Fig. 5.11 obtained through the lagrangian sensor).
- The strain field analysis permits other remarks concerning the adequacy of tensile test for the workability investigation:
- even if the strain field is mainly compressive, the deformation component along the x axis has a positive peak value on the expected crack region (Fig. 5.12a);
- strain value along the x axis (corresponding to the direction in which the first principal stress component acts) at the minimum rolls gap (Fig. 5.12a) is comparable with the strain at fracture determined in experimental tests in central material (Fig. 4.12);
- numerical prediction of the strain rate field in the billet axis zone (Fig. 5.12b, even if in equivalent terms) confirms the adequacy of the strain rate

condition assumed for the experimental tensile test campaign.

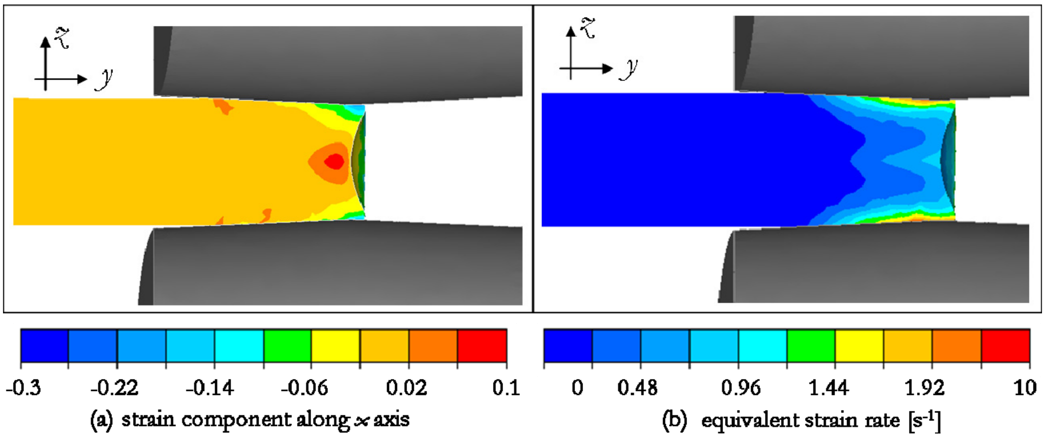

Fig. 5.12 Strain along x axis and equivalent strain rate distributions

5.3.2 Damage models' capabilities on the Mannesmann effect identification

Three different approaches to fracture prediction were tested in the preliminary numerical model, according to what was found in literature review. This first damage implementation was used to identify which of the different approaches would have been the most appropriate in the description of the Mannesmann effect.
The main focus with this basis was to correctly reproduce the fracture site of the real case and then accurately calibrate the best model. In view of this objective and in order to shorten the sensitivity analysis step, coupling between material rheology and damage was not introduced and rough data was used for the necessary material dependent damage parameters.
Different Mannesmann fracture site predictions according to the approaches chosen will be presented in the following.
Every observation will be made at the same time increment in the simulation corresponding to the working zone in which the billet should start to fracture in the industrial conditions. Thanks to a yz cutting plane containing the billet axis, the damage accumulation in the theoretical real fracture site can be shown.

As reported in the second chapter, an energy-based approach and, in particular, the Cockcroft & Latham damage model, is probably the most implemented damage model in forming numerical simulations (eq. V.1). The prediction of the Mannesmann effect adopting this formulation is reported in Fig. 5.13: it is evident that the model is not able to correctly describe the damage distribution since it predicts the maximum damaged zone on the external surface of the billet.

$$D = \int_{0}^{\varepsilon_f} \sigma_1 d\varepsilon \qquad \text{(V.1)}$$

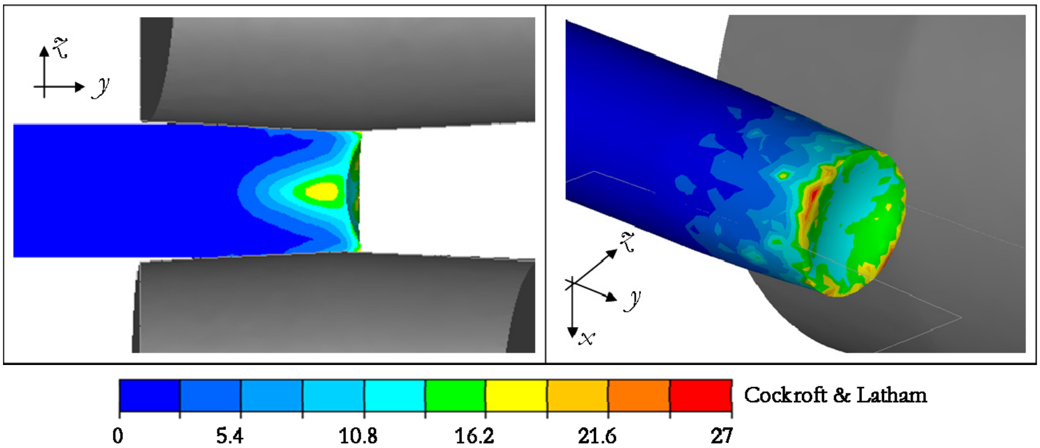

Fig. 5.13 Cockcroft & Latham damage prediction

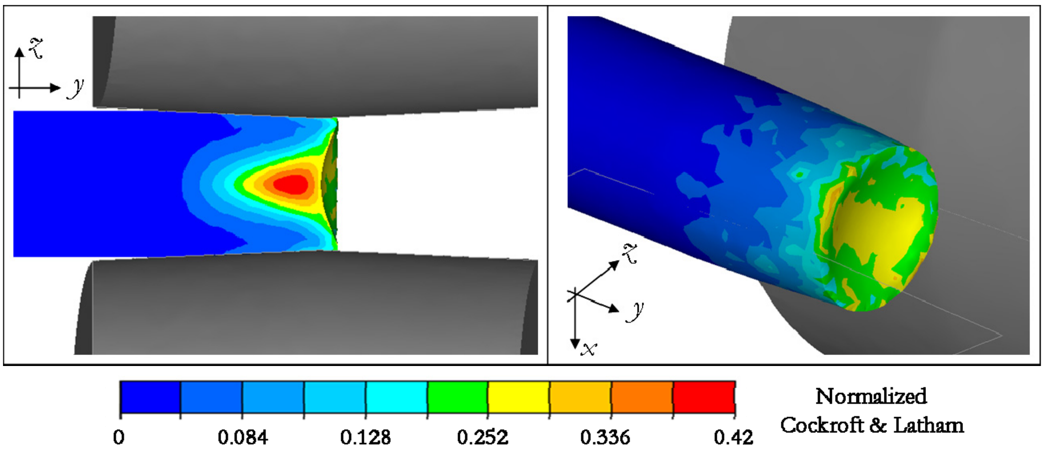

Fig. 5.14 Normalized Cockcroft & Latham damage prediction

A better damage prediction can be made by implementing the normalized version of the Cockcroft & Latham model (eq. V.2, Fig. 5.14). In fact, damage accumulation in the axis zone of the billet (*yz* cutting plane) is more representative of the Mannesmann effect than the simple formulation.

$$D = \int_0^{\varepsilon_f} \frac{\sigma_1}{\bar{\sigma}} d\bar{\varepsilon} \qquad \text{(V.2)}$$

The Oyane damage model, being based on void growth micro-mechanics, was tested in order to improve the prediction of a fracture site with respect to the previous results (eq. V.3, Fig. 5.15, parameter *B*=3). The outer surface of the billet is characterized by a particularly lower damage value with respect to the Cockcroft & Latham models.

$$D = \int_0^{\varepsilon_f} 1 + B\frac{\sigma_H}{\bar{\sigma}} d\bar{\varepsilon} \qquad \text{(V.3)}$$

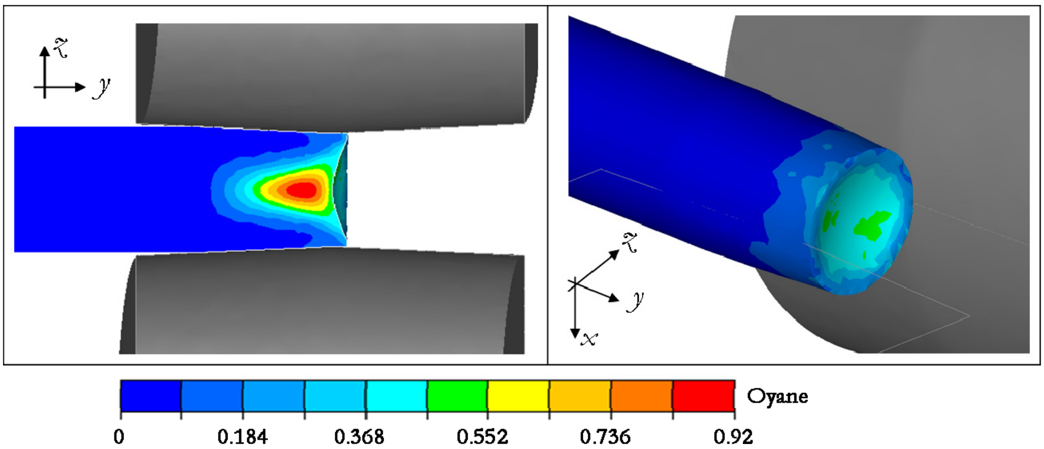

Fig. 5.15 Oyane damage prediction

The best fracture site prediction, in this preliminary context, was obtained using the Continuum Damage Mechanics and implementing a simplified formulation for proportional loading condition of the Lemaitre theory (Tab. 5.3, without coupling with rheology, void closure effect and triaxiality cut-off value) [71].

The damage concentration on the billet axis is well defined observing the distribution on the *yz* cutting plane and the outer surface of the billet is in practice undamaged as in the real case (Fig. 5.16).

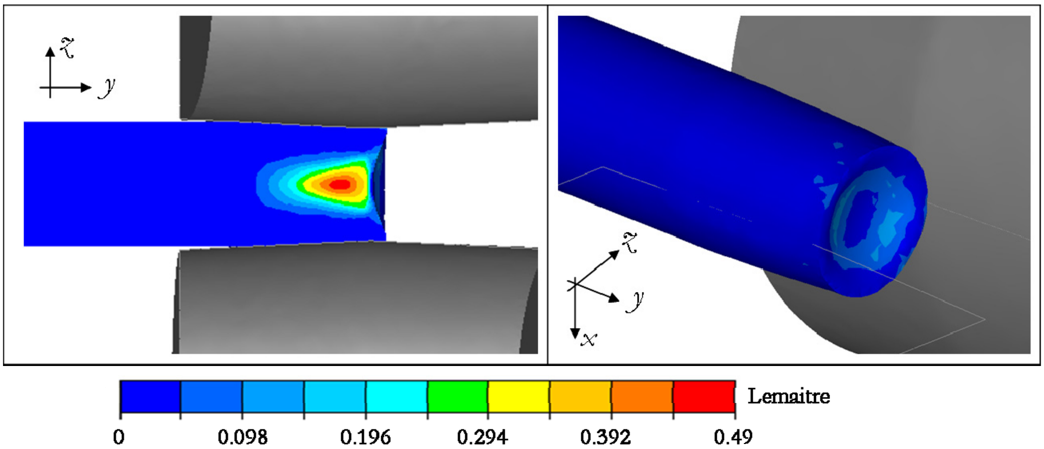

Fig. 5.16 Lemaitre damage prediction

$\sigma_D = (1-D)\sigma$ EFFECTIVE STRESS
If $\left(\sigma_H < 0, \bar{\sigma} \neq 0, \bar{\varepsilon} > \varepsilon_{th}\right)$ then $\left\{ \begin{array}{l} R_V = \frac{2}{3}(1+\nu) + 3(1-2\nu)\frac{\sigma_H^{\;2}}{\bar{\sigma}^2} \\ \frac{\partial D}{\partial t} = \frac{D_C}{(\varepsilon_R - \varepsilon_{th})} R_V \dot{\bar{\varepsilon}} \end{array} \right\}$ otherwise $\frac{\partial D}{\partial t} = 0$

Tab. 5.3 Lemaitre standard formulation for proportional loading

The adequacy of Lemaitre's model on fracture prediction can be justified by the role that the stress triaxiality holds in the formulation. In fact, unlike the other tested approaches, the explicit presence of the triaxiality function R_V on the model makes it possible to distinguish the role of the compressive deformation at the outer surface on the damage growth with respect to the tensile one towards the axis (Fig. 5.9-5.11).

5.4 CONCLUSION

- The developed numerical model of the non-plug piercing operation was tested and some remarks can be made:
- the rolling of the cylindrical billet was carried out on the commercial code Forge® and it can replicate the deformation history that characterizes the real industrial case;
- the accuracy obtained on the prediction of the stress and strain fields made it possilbe to analyse the conditions characterizing the Mannesmann effect;
- the implementation of different damage models approaching fracture differently, made it possible to evaluate the most adequate one with regards to the description of the critical conditions for the formation of the crack due to the Mannesmann effect.

CHAPTER 6

ENHANCEMENT OF THE LEMAITRE DAMAGE MODEL

6.1 INTRODUCTION

In view of the results on the damage models capability to represent the Mannesmann effect, the Lemaitre model was definitely chosen for the fracture prediction. A modification of the standard model was made in order to take into account the main experimental issues regarding initial voids and phase distributions on the initial billet that affect the fracture behavior of the material.
The identification of the material dependent damage parameters required the development of the numerical model of the hot tensile test and inverse analysis technique applied to the experimental data.

6.2 IMPLEMENTATION OF THE LEMAITRE DAMAGE MODEL

The complete Lemaitre formulation according to the presentation given in section 2.2.3.4 will be adopted.
From the numerical point of view, coupling between mechanical properties and damage was adopted as well. Following the definition of weak coupling, the damage parameter *D* computed at the generic time *t* is considered in the computation of material properties at time *t+dt*, in particular the effective Young modulus and the effective stress are calculated:

$$E_{EFF,t+dt} = E_{t+dt}(1 - D_t) \quad \text{(VI.1)}$$

$$\sigma_{EFF,t+dt} = \frac{\sigma_{t+dt}}{1 - D_t} \quad \text{(VI.2)}$$

The determination of the material dependent parameters introduced in section 2.2.3.4 are required to calibrate the damage model. A numerical model of the tensile test on Gleeble® conditions was developed and inverse analysis on experimental results was performed for the damage parameters identification (D_C, S_0, s).

6.2.1 Numerical simulation of the hot tensile test

A two dimensional numerical model of the tensile test was developed using Forge®, reproducing the thermal and mechanical conditions realized in the Gleeble® chamber during the experimental campaign (Fig. 6.1).

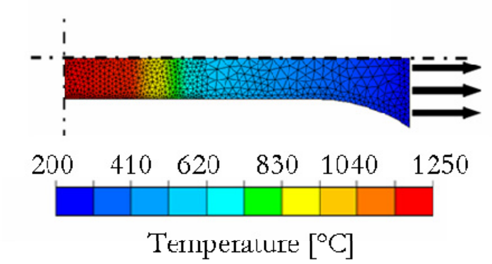

Fig. 6.1 Initial temperature distribution on the gage length of the tensile sample

Several thermocouples were placed on the tensile sample and the typical temperature profile due to the resistance heating system was reported in the initial condition of the two dimensional numerical model. This setting made it possible to accurately reproduce the necking phase during the test.
Considering the direction of the secondary tensile stress component characterizing the typical state of stress of the Mannesmann effect, experimental tests on samples normal to the billet axis were considered to calibrate the damage model.
First, material damage parameters were determined from the tensile test results on peripheral material in view of their ample availability, the lower uncertainty and the negligible amount of voids on the peripheral region. An automatic procedure was established to compare experimental and numerical force/displacement curves in which 150 iterations were performed before accepting the fitted damage parameters.
Tab. 6.1 collects the identified parameters in which the void closure factor h_C was maintained constant and equal to 0.2 according to the Lemaitre guideline [21].

D_C	S_0	s	ε_{th}	h_C
0.58	1.2198	0.3985	0.01	0.2

Tab. 6.1 Material dependent damage parameters for the Lemaitre model

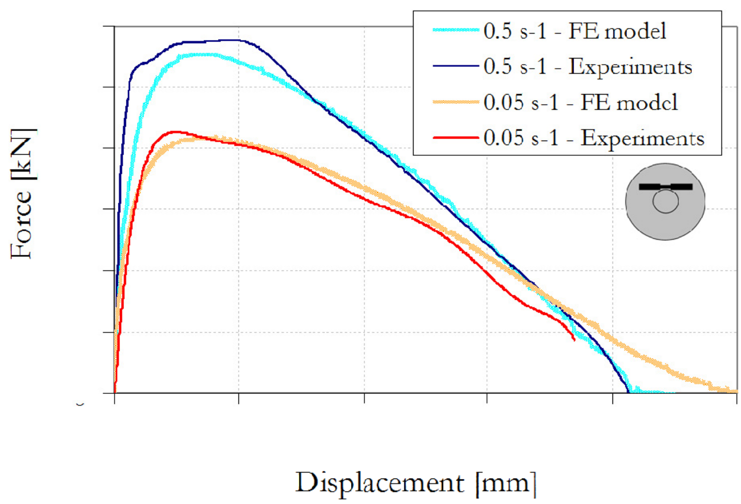

Fig. 6.2 Prediction of peripheral material response for different strain rate condition

The comparison between the experimental tensile test results and the

numerical prediction obtained with the implementation of the calibrated damage model is reported in Fig. 6.2. In addition, it was verified, as shown in Fig. 6.2, that the identified parameters are not strain rate dependent: in fact there is also a good prediction of peripheral material response when the tensile test velocity is varied.
The so calibrated damage model could no longer be implemented on the numerical simulation of non-plug piercing for the prediction of Mannesmann fracture conditions. In fact, at this point, the standard formulation only described the fracture behaviour of the peripheral material that is the portion least affected by the solidification after casting. A modification of the standard formulation was required in order to model the fracture behaviour of the entire billet material and this way increase the accuracy of the numerical simulation. The modification mainly considers the distribution of mechanical properties on the billet section due to the micro-structural characteristics discussed in chapter 4 of this work.

6.2.2 Modification of the standard Lemaitre model

1) The need to modify the damage law is related to the modelling of two fundamental aspects observed through the experimental campaign on the material (Fig. 6.3):
2) material at the billet centre has a lower maximum tensile stress with respect to the peripheral one;
3) the central region of the billet has a lower fracture strain than the periphery.

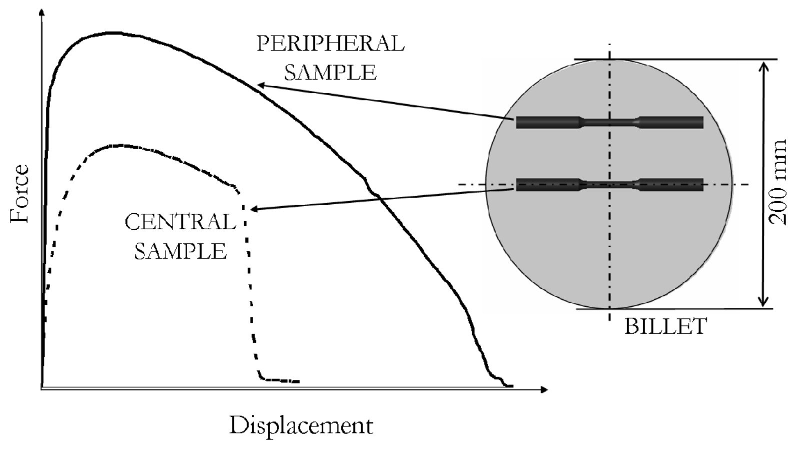

Fig. 6.3 Material properties dependency on radial location on the billet section

These two material characteristics derive from the non-homogeneity of the cooling phase after casting; from the damage point of view they can be expressed as:

1) a non-zero initial damage value dependent on the radial location of the material and directly related to the void content and phase distribution measured with the metallographic technique (section 4.3.3);
2) an increase of the damage rate from the periphery towards the billet centre in view of the observed lower fracture limits.

In order to fulfil these requirements, an additional parameter $D_{in}(r)$, function of the radial position r on the billet section and representing initial damage, and a modification of the damage rate were introduced.

These new assumptions made it possible to characterize the damage behaviour of the central material using the damage parameters determined on the peripheral one. The schematization in Fig. 6.4 makes the concept explanation easier.

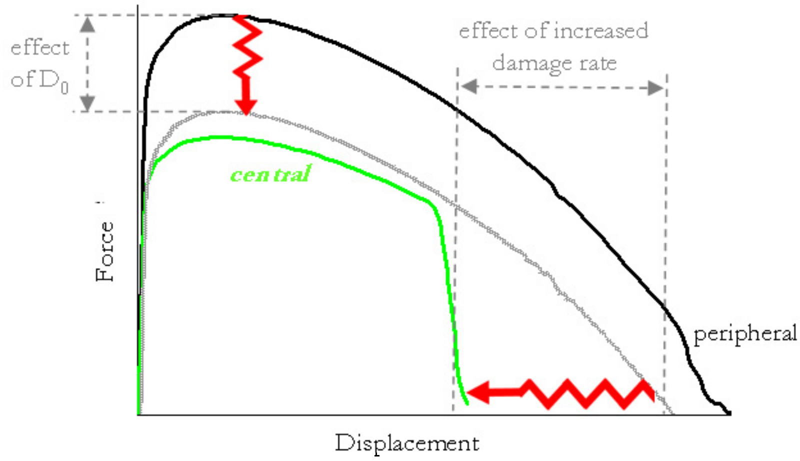

Fig. 6.4 Schematization of the modifications introduced into the damage model

The damage model modification involved especially the central zone of the initial billet in view of the results from micro-structural analysis (section 4.3.3). As a consequence, the peripheral material was chosen as effectively representing the undamaged material condition (D_{in}=0).

The maximum value of the initial damage $D_0 = D_{in}(r=0)$, corresponding to the material on the axis, was determined through inverse analysis applied to the central sample tensile test data. The radial distribution law of initial damage was defined combining the inverse analysis on central samples (for the value of D_0) and the voids gradient detected by micro-structural investigation (for the exponential radial trend, Fig. 6.5, represented by the exponent of the law).

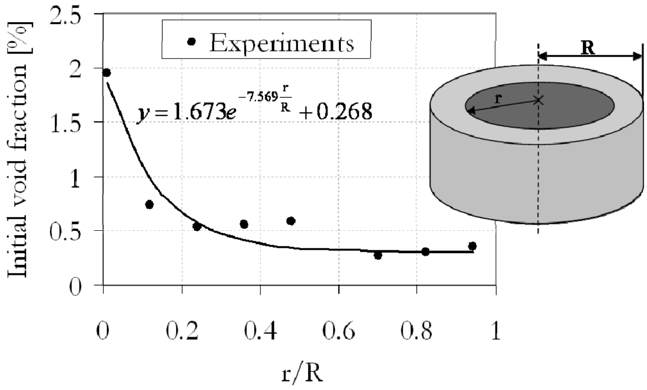

Fig. 6.5 Exponential trend of the void content

The exponential law in equation VI.1, expressed with respect to the billet radius R, reports the initial damage distribution that was implemented in the simulation for the billet material (Fig. 6.6):

$$D_{in} = 0.2 \cdot e^{\left[-7.569\left(\frac{r}{R}\right)\right]} \qquad \text{(VI.1)}$$

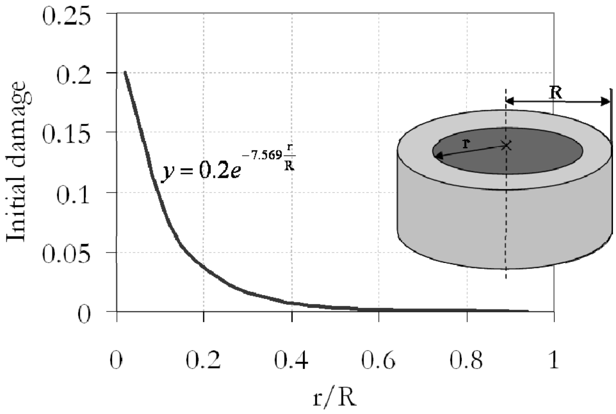

Fig. 6.6 Initial damage dependence on the radial position on the billet

The influence of initial material properties on the damage evolution law was taken into account introducing the new parameters D_{in} and s_2 (both obtained

through inverse analysis on axial samples tensile test results) in order to relate the effect of micro-structural non-homogeneity to the damage exponent *s*. In view of the initial damage definition (eq. VI.1), the damage rate has become dependent on the radial position on the billet *r* and hence it can represent more accurately the real damage evolution which is characterized by the influence of local voids content and phase distribution.
The modified formulation for the damage rate is reported in equation VI.2 and VI.3, referring to a positive and a negative triaxiality state of stress respectively, as mentioned in section 2.2.3.4.

$$\dot{D} = \left(-\frac{Y}{S_0} \right)^{s - s_2 D_0} \dot{\bar{\varepsilon}} \qquad \text{(VI.2)}$$

$$\dot{D} = \left(-\frac{h_C Y}{S_0} \right)^{s - s_2 D_0} \dot{\bar{\varepsilon}} \qquad \text{(VI.3)}$$

New equations expressing initial damage and modified damage rate law were implemented into the numerical code Forge® compiling a proper user subroutine and the initial damage distribution that was set on the billet is reported in Fig. 6.7.

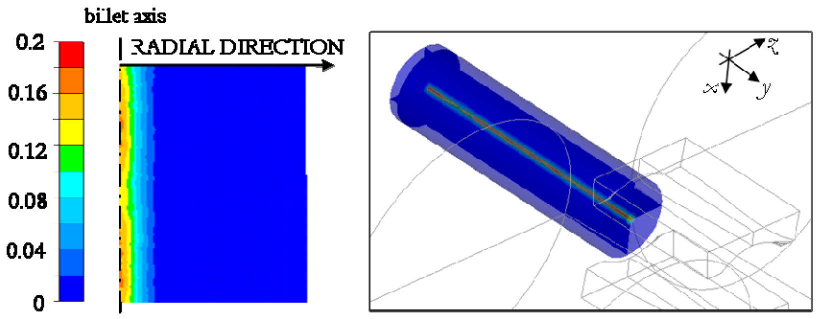

Fig. 6.7 Initial damage radial distribution on the FE model

Applying this damage distribution and performing some computations, remeshing in the billet was definitely removed from the simulation set up since it induced a sort of homogenization of the damage field during the deformation, hence an accurate prediction would be impossible.

6.3 FINAL CALIBRATION OF THE DAMAGE MODEL

According to Lemaitre's observations, traditional damage parameters S_0, s and D_C must be considered as material dependent, hence the same for peripheral and central material.
Once the standard Lemaitre formulation was modified, damage parameters previously determined studying the peripheral material were maintained and inverse analysis was necessary to identify the maximum amount of initial damage D_0 and the value of the parameter s_2 of the evolution law exponent. These particular values are characteristic of the experimental response from the tensile test of the billet centre material (Tab. 6.2).

D_C	S_0	s	s_2	ε_{th}	h_C	$D_0(r=0)$
0.58	1.2198	0.3985	1.5	0.01	0.2	0.2

Tab. 6.2 Damage parameters for the material on the billet axis zone

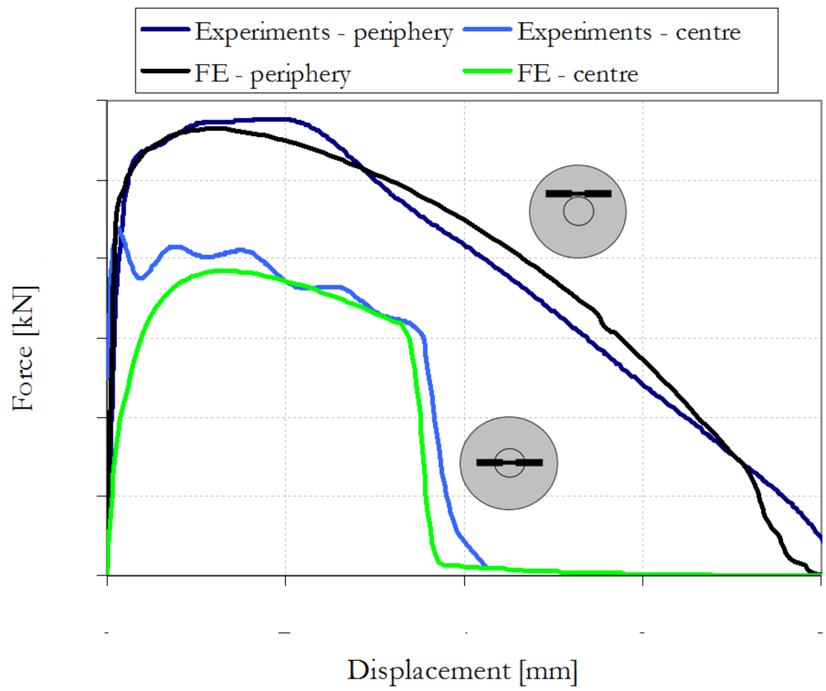

Fig. 6.8 Modelling the hot tensile test thanks to the calibrated damage model

Numerical prediction of the material tensile response is shown in Fig. 6.8:

introducing the concept of initial damage and modifying the damage rate according to equation VI.2, the modelling of the entire billet material behaviour was possible.

6.4 CONCLUSION

The standard formulation of the Lemaitre damage model implies the homogeneity of the material in terms of mechanical properties.
Due to the evident differentiation of the material behaviour observed on the continuously cast billet, the modelling of the material fracture behaviour required a modification of the original damage law introducing the concept of initial damage and taking into account the influence of the billet micro-structural properties due to the solidification after casting.
The new damage formulation was obtained independently from the Mannesmann effect conditions. The model conception and calibration phases were based on experimental observations of the material and standard laboratory testing procedures. The introduction of the initial damage concept as well as the modification of the damage rate law made the modelling of the entire billet material behaviour possible.

CHAPTER 7

NUMERICAL PREDICTION OF THE MANNESMANN FRACTURE

7.1 INTRODUCTION

Once the proposed damage model was properly calibrated, it was implemented into the numerical simulation of the non-plug piercing operation compiling an external user routine for the three dimensional code.
A weak coupling approach was followed on the material behavior representation; material fracture due to the Mannesmann effect was numerically obtained adopting the kill element technique on the mesh elements in which computed Lemaitre damage reaches the critical value D_C determined through experiments.
Mannesmann fracture was modeled and final agreement between numerical

estimation and industrial results was obtained.

7.2 NUMERICAL RESULTS WITH THE ENANCHED DAMAGE MODEL

7.2.1 Improvement on the damage prediction

The new D_{in} parameter introduced in the damage model made it possible to correctly describe the damage evolution in the central region of the billet. The improvement in the modelling due to the modification of the damage rate in dependency of initial damage value appears evident observing the damage prediction obtained thanks to a lagrangian sensor on the expected cracking zone (Fig. 7.1):

- the standard formulation of the damage law, not taking into account the lower strength of the central billet material, was not able to describe the arrival point of the critical condition in the region in which the fracture was expected;
- thanks to the modifications related to the concept of initial damage, the new formulation proposed for the Lemaitre model better represented the damage evolution in the billet section and made it possible to reach the fracture condition as expected when the billet came near the minimum rolls gap.

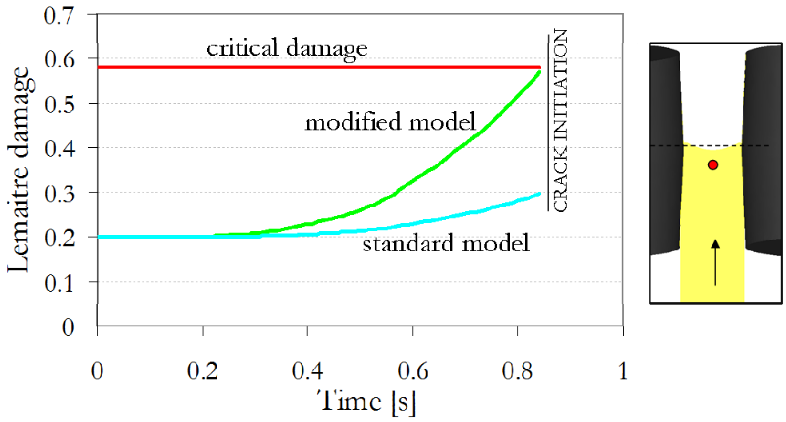

Fig. 7.1 Damage evolution at the crack initiation site (lagrangian sensor)

7.2.2 Mannesmann crack features

As soon as the critical condition for fracture is reached ($D=D_C$), Mannesmann crack was reproduced in the FE model by using the kill element technique (the critical damage value was reached at process time actually equal to 0.9 s, Fig. 7.2). Very fine mesh on the cracking region is a fundamental requirement of the numerical model in order to avoid the creation of an excessively extended fracture and hence an incorrect estimation (as explained in chapter 5, average mesh element size on the axis zone has to be as low as possible).
Two different aspects have to be modelled with the fracture reproduction:
- the initiation site, where the first element reaches the critical damage value;
- the crack propagation, all the elements with damage higher than the critical value are deleted.

Fig. 7.2 resumes the numerical damage field (Lemaitre modified formulation) at process time of 0.9 s (crack initiation) and 1.5 s (stop of the crack propagation – end of the simulation).

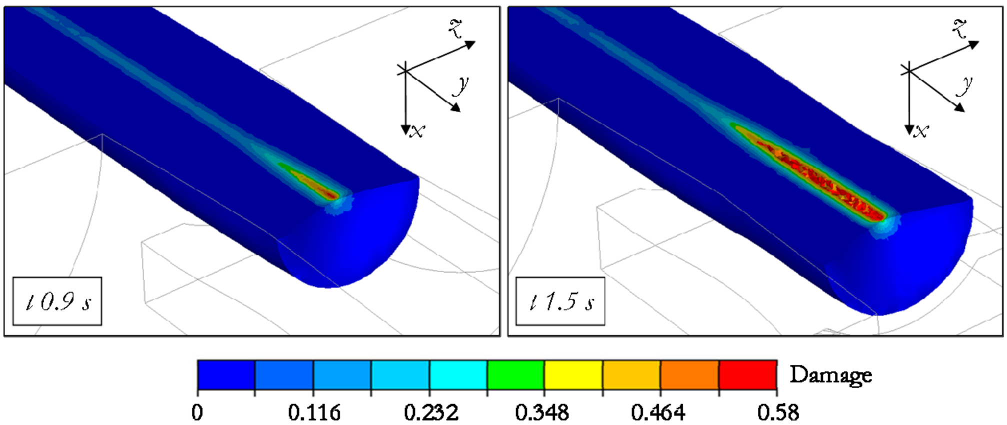

Fig. 7.2 Damage distribution at crack initiation and at the last computed increment

From the industrial point of view, the reference for the fracture length measurement is usually the minimum rolls gap, or rather the position on which the billet is submitted to the maximum squeezing.
Two features were taken into account for the evaluation of the model capability on the prediction of the Mannesmann fracture:
1) length of the crack, represented by the distance of the crack tip from the minimum rolls gap;
2) the crack thickness that is represented by its extension on the direction

normal to the rolling one.
The experimental measurement of the Mannesmann length obtained through the industrial trial was possible using a longitudinal section on the partially rolled billet (referring to the condition of industrial test n. 4, see Tab. 4.1). The fracture cone tip position with respect to the minimum rolls gap is shown in Fig. 7.3. The measured length of the Mannesmann cone was equal to 100 mm.

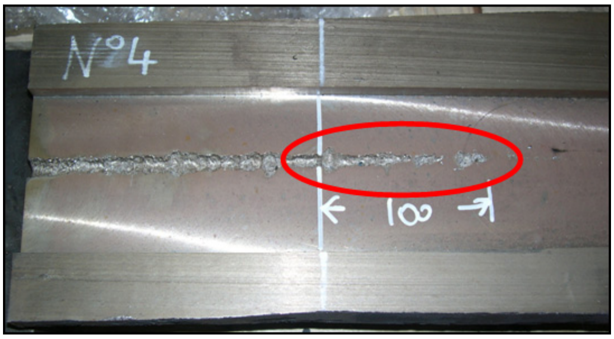

Fig. 7.3 Mannesmann fracture on industrial trial n. 4

Concerning the numerical prediction, the damage calculation made it possible to identify the crack initiation after 0.9 s from the process beginning, at 15 mm before the minimum rolls gap (Fig, 7.4a).

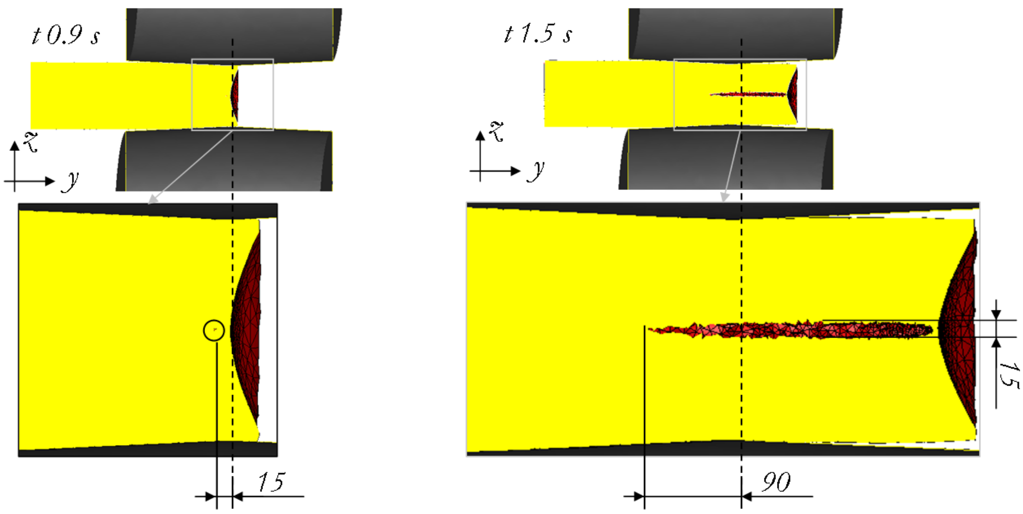

(a) (b)

Fig. 7.4 Numerical prediction of the Mannesmann fracture

Continuing the deformation after the crack initiation, the Mannesmann cone vertex moves from the initiation site (15 mm) to 90 mm from the minimum rolls gap. This result is reported in Fig. 7.4b.
The final increment, computed after 1.5 s from the process beginning, was chosen as the end of the simulation in view of the stationary condition reached by the Mannesmann cone. In fact, the numerical propagation of fracture is associated to the backward movement of the cone tip until a sort of equilibrium from an eulerian point of view is reached, corresponding to a crack length of 90 mm from the roll gap.
This stationary state of the deformation corresponds to the state of the semi-rolled billet obtained in the industrial trials and good agreement can be observed between the real crack length and the predicted one.
The prediction of the fracture width is also satisfactory: in fact the 15 mm value obtained through the numerical model (fig. 7.4b) totally agrees with a direct measurement of the same amount on the sectioned semi-rolled part.

7.2.3 Geometrical features of the semi-rolled part

- The numerical simulation developed has also been able to predict with good accuracy the main geometrical features of the semi-rolled part (Fig. 7.5):
- the model can correctly reproduce the concave shape on the frontal surface of the billet;
- the damage model catches the aspect where the Mannesmann fracture initiation site is located inside the part and no fracture occurs on the frontal surface.

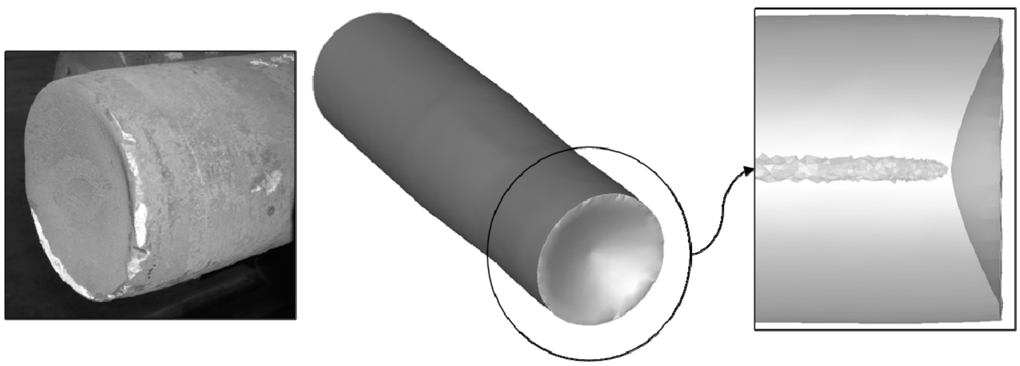

Fig. 7.5 Top surface of the partially rolled billet

7.3 CONCLUSION

- The implementation of the modified Lemaitre damage model in the numerical simulation made the prediction of the Mannesmann fracture formation conditions possible:
- the proposed modification of the damage model was validated, the improvement on the fracture prediction developed under tensile test conditions was successfully applied to the prediction of the crack due to the Mannesmann effect;
- the main characteristics of the crack were reproduced numerically, length and width of the Mannesmann cone were considered satisfactory if compared with their direct measurement on the semi-rolled billet obtained in the industrial forming conditions.

CHAPTER 8

CONCLUSIONS

In order to predict the central fracture due to the Mannesmann effect in the steel piercing process, an approach based on the combination of experimental and numerical techniques was proposed to fulfil the objective.
The workability of a steel commonly applied for tube production and obtained through continuous casting was investigated using laboratory testing techniques. The main results can be summarized as follows:

- the mechanical properties of the cylindrical billet are strongly dependent on the radial distance from its centre, as shown by the results of hot tensile tests under process conditions;
- the considerably high voids content and ferritic phase concentration, identified through metallographic analyses, are two of the main aspects that influence the low strength that characterizes central billet material.

A three-dimensional FEM model of the Mannesmann piercing process without the plug was developed in order to identify the strain and stress states at the billet axis.

As the cavity initiation for Mannesmann effect seemed to be mainly induced by the secondary tensile stress (first principal component of stress), the hot tensile test was confirmed to be an appropriate method to evaluate material workability.
Continuum Damage Mechanics was proved to be an appropriate approach to describe the fracture formation under the Mannesmann effect conditions and it was integrated into the numerical model of the non-plug piercing according to the Lemaitre formulation.
In order to correctly describe the damage history of the billet material, it was necessary to modify the Lemaitre model introducing the initial damage concept into the model itself. This made it possible to take into account the distribution of the mechanical properties on radial direction of the billet continuously cast material.
The damage model required an accurate calibration phase before its implementation into the numerical simulation of the non-plug piercing operation: a numerical model of the tensile test condition was developed and the necessary material dependent damage parameters were determined using inverse analysis technique on experimental tensile test results.

The validation of the numerical simulation was made by comparing the Mannesmann fracture numerical prediction with the measurements on non-plug piercing trials carried out on an industrial mill.
The developed numerical model was able to correctly describe the central crack due to the Mannesmann Effect; some significant comments about obtained results are the following:
- the crack initiation position is close to the minimum rolls gap and the Mannesmann cone tip moves back until a sort of stationary condition is reached during the deformation process;
- the crack initiation position should be strongly influenced by boundary effects in the front section of the billet; this numerical result, however, is difficult to validate with experimental trials due to the difficulty in stopping the mill right at the billet entrance.

The proposed approach has proved to be a suitable technique for the correct process design before starting production:
- using the numerical simulation, the position of the mandrel on the piercing mill can be chosen thanks to the knowledge of the Mannesmann cone length without expensive preliminary industrial trials;
- the material dependent damage parameters can be identified coupling hot

tensile test results with metallographic observations and inverse analysis techniques.
- the calibration of the numerical model can be done on the basis of simple laboratory tests under process conditions.

The effective prediction of fracture due to the Mannesmann effect was, up til now, lacking in technical-scientific literature. Before the study carried out in this work, several numerical models of the piercing process were developed but there was no model able to completely describe the initiation and propagation of the crack in the process conditions.
The innovative and fundamental aspect of this study is the key role that the continuously cast material properties distribution plays in the damage model; the possibility of their determination through simple laboratory techniques makes the proposed approach easy to implement for different materials and working conditions.

REFERENCES

[1] M. G. Cockcroft, D. J. Latham, *Ductility and the Workability of Metals*. J. Inst. Met. 96 (1968) 33.

[2] G. E. Dieter, *Workability Testing Technique*. American Society for Metals, 1984.

[3] F. A. McClintock, *A Criterion for Ductile Fracture by the Void Growth*. Trans. ASME, J. Appl. Mech. 17 (1968) 363.

[4] J. R. Rice, D. M. Tracey, *On the Ductile Enlargement of Voids in Triaxial Stress fields*. J Mech Phys Solids 17 (1969)201.

[5] M. Oyane, *Criteria For Ductile Fracture Strain*. Bull. JSME 15 (1972) 1507.

[6] A. G. Atkins, E*lastic and Plastic Fracture*. Wiley, New York, 1985

[7] Y. Bao, T. Wierzbicki, *On fracture locus in the equivalent strain and stress triaxiality space*. International Journal of Mechanical Sciences 46 (2004) 81-98.

[8] Y. Bao, *Dependence of ductile crack formation in tensile tests on stress triaxiality, stress and strain ratios*. Journal of Engineering Fracture Mechanics 72 (2005) 505-522.

[9] Y. Bao, T. Wierzbicki, *On the cut-off value of negative triaxiality for fracture*. Journal of Engineering Fracture Mechanics 72 (2005) 1049-1069.

[10] F. A. Freudenthal, *The Inelastic Behaviour of Solids*. Wiley, New York (1950).

[11] P. Brozzo, B. Deluca, R. Rendina, *A New Method for the Prediction of Formability Limits in Metal Sheets, Sheet Metal Forming and Formability*. Proceedings of the Seventh Biennial Conference of the International Deep Drawing Research Group, 1972.

[12] J. W. Hancock, A. C. Mackenzie, *On the Mechanisms of Ductile Failure in High-strength Steels Subjected to Multi-axial Stress-states*. J. Mech. Phys. Solids 24 (1976) 147-169.

[13] M. Oyane, T. Sato, K. Okimoto, S. Shima, *Criteria for Ductile Fracture and Their Application*. Journal of Mechanical Working Technology 4 (1980), 65-81

[14] A. Gurson, *Continuum Theory of Ductile Rupture by Void Nucleation and Growth: Part I – Yield Criteria and Flow Rules for Porous Ductile Media*. J. Engng Mater Technol 99 (1977) 2.

[15] V. Tvergaard, *Influence of Voids on Shear Band Instabilities Under Pane Strain Conditions*. Int J Fract 17 (1981) 389.

[16] V. Tvergaard, A. Needleman, *Analysis of Cup-cone Fracture in Round Tensile Bar*. Acta Metall 32 (1984) 157.

[17] L. M. Kachanov, *Time of the Rupture Process Under Creep Conditions*. Izv. A.N.SSSR, Otd. Tekh. Nauk, 8 (1958) 26-31.

[18] J. Lemaitre, *How to Use Damage Mechanics*. Nuclear Engineering and Design 80 (1984) 233-245.

[19] J. Lemaitre, *A Continuous Damage Mechanics Model for Ductile Fracture*. Journal of Engineering Materials and Technology, 107 (1985) 83-89.

[20] J. Lemaitre, J. P. Sermage, *One Damage Law for Different Mechanisms*, Computational Mechanics 20 (1997) 84-88.

[21] J. Lemaitre, R. Desmorat, *Engineering Damage Mechanics*. Springer-Verlag, Berlin, 2005.

[22] N. Bonora, *A Nonlinear CDM Model for Ductile Failure*, Engineering Fracture Mechanics 58-1 (1997) 11-28.

[23] N. Bonora, D. Gentile, A. Pirondi, G. Newaz, *Ductile Damage Evolution Under Triaxial State of Stress: Theory and Experiments*, International Journal of Plasticity 21 (2005) 981-1007.

[24] N. Bonora, A. Ruggiero, L. Esposito, D. Gentile, *CDM Modelling of Ductile Failure in Ferritic Steels: Assessment of the Geometry Transferability of Model Parameters*, International Journal of Plasticity 22 (2006) 2015-2047.

[25] S. E. Clift, P. Hartley, C. E. N. Sturgess and G. W. Rowe, *Fracture Prediction in Plastic Deformation*. International Journal of Mechanical Sciences 32 (1990) 1-17.

[26] B.P.P.A. Gouveia, J.M.C. Rodrigues, P.A.F. Martins, *Fracture Predicting in Bulk Metal Forming.* International Journal of Mechanical Sciences 38-4 (1996) 361-372.

[27] B.P.P.A. Gouveia, J.M.C. Rodrigues, P.A.F. Martins, *Ductile Fracture in Metalworking: Experimental and Theoretical Research* Journal of Materials Processing Technology 101 (2000) 52-63.

[28] J. Landre, A. Pertence, P. R. Celtin, J.M.C. Rodrigues, P.A.F. Martins, *On the Utilisation of Ductile Fracture Criteria in Cold Forging* Journal of Finite Elements in Analysis Design 39 (2003) 175-186.

[29] M. Simionato, A. Ghiotti, S. Bruschi, *Billet Cropping Numerical Modelling: an Approach Based on Inverse Analysis*, International Journal of Material Forming, Springer/ESAFORM2008 (2008).

[30] T. Wierzbicki, Y. Bao, Y.W. Lee, Y. Bai, *Calibration and Evaluation of Seven Fracture Models.* International Journal of Mechanical Sciences 47 (2005) 719-743.

[31] I. M. Pereira, G. Rubim, O. Acselrad, P. R. Celtin, *Comparison of the Experimental and the Numerically Predicted Mechanical Damage in the Sheet Forming of Steel.* Journal of Materials Processing Technology 203 (2008) 13-18.

[32] E. Taupin, J. Breitling, W. T. Wu and T. Altan, *Material Fracture and Burr Formation in Blanking Results of FEM Simulations and comparison with experiments.* Journal of Materials Processing Technology 59 (1996) 68-78.

[33] N. Schluter, F. Grimpe, W. Bleck, W. Dahl, *Modeling of the Damage in Ductile Steels.* Computational Material Science 7 (1996) 27-33.

[34] M. Rakin, Z. Cvijovic, V. Grabulov, S. Putic, A. Sedmak, *Prediction of Ductile Fracture Initiation Using Micromechanical Analysis.* Engineering Fracture Mechanics 71 (2004) 813-827

[35] M. Springmann, M. Kuna, *Identification of Material Parameters of the Gurson-Tvergaard-Needleman Model by Combined Experimental and Numerical Techniques.* Computational Materials Science 33 (2005) 501-509.

[36] K. Komori, *Effect of Ductile Fracture Criteria on Chevron Crack Formation and Evolution in Drawing.* International Journal of Mechanical Sciences 45 (2003) 141-160.

[37] V. Uthaisangsuk, U. Prahl, S. Munstermann, W. Bleck, *Experimental and Numerical Failure Criterion for Formability Prediction in Sheet Metal Forming.*

Computational Materials Science 43 (2008) 43-50.

[38] R. Hambli, *Finite Element Model Fracture Prediction During Sheet-Metal Blanking Processes*, Engineering Fracture Mechanics 68 (2001) 365-378.

[39] R. Hambli, A. Mkadem, A. Potiron, *Finite Element Modeling in Bending Processes*, Journal of Materials Processing Technology 147 (2004) 302-310.

[40] A. Mkaddem, F. Gassara, R. Hambli, *A New Procedure Using the Microhardness Technique for Sheet Material Damage Characterization*, Journal of Materials Processing Technology 178 (2006) 111-118.

[41] F. M. Andrade Pires, J. M. A. César de Sà, L. Costa Sousa, R. M. Natal Jorge, *Numerical Modelling of Ductile Plastic Damage in Bulk Metal Forming*, International Journal of Mechanical Sciences 45 (2003) 273-294.

[42] F. M. Andrade Pires, E. A. De Souza Neto, D. R. J. Owen, *On the Finite Element Prediction of Damage Growth and Fracture Initiation in Finitely Deforming Ductile Materials*, Comput. Methods Appl. Mech. Engrg. 193 (2004) 5223-5256.

[43] P. Teixeira, A. D. Santos, F. M. Andrade Pires, J. M. A. César de Sà, *Finite Element Prediction of Ductile Fracture in Sheet Metal Forming Processes*, Journal of Materials Processing Technology 177 (2006) 278-281.

[44] J. M. A. César de Sà, P. M. A. Areias, Cai Zheng, *Damage Modelling in Metal Forming Problems Using an Implicit Non-Local Gradient Model*, Comput. Methods Appl. Mech. Engrg. 195 (2006) 6646-6660.

[45] A. Behrens, H. Just, *Extension of the Forming Limits in Cold and Warm Forging by the FE Based Fracture Analysis with the Integrated Damage Model of Effective Stresses*, Journal of Materials Processing Technology 125-126 (2002) 235-241.

[46] A. Behrens, H. Just, *Verification of the Damage Model of Effective Stresses in Cold and Warm Forging Operations by Experimental Testing and FE Simulations*, Journal of Materials Processing Technology 125-126 (2002) 295-301.

[47] P. O. Bouchard, T. Laurent, L. Tollier, *Numerical Modelling of Self-Pierced Riveting - From Riveting Process Modelling Down to Structural Analysis*, Journal of Materials Processing Technology 202 (2008) 290-300.

[48] P. D. Nicolaou, S. L. Semiatin, *An Experimental and Theoretical Investigation of the Influence of Stress State in Cavitation During Hot Working*. Acta

Materialia 51 (2003) 613-623.

[49] D. C. J. Farrugia, *Prediction and Avoidance of High Temperature Damage in Long Product Hot Rolling*, Journal of Materials Processing Technology 177 (2006) 486-492.

[50] W. A. Khudheyer, D. C. Barton, T. Z. Blazynski, *Pass Geometry and Macroshear Redundancy Effects in a 3-Roll Conical Oblique Tube Piercing Process*, Journal of Materials Processing Technology 45 (1994) 341-345.

[51] E. Erman, *The influence of the Processing Parameters on the Performance of the Two-Roll Piercing Operation*, Journal of Mechanical Working Technology 15 (1987) 167-179.

[52] C. Hayashu, T. Yamakawa, *Influences of Piercing Ratio, Expansion Ratio, Feed, Cross and Skew Angles on Available Piercing Size Range in Rotary Piercing Process*, ISIJ International 38-11 (1998) 1255-1261.

[53] S. Urbanski, J. Kazanecki, *Assessment of the Strain Distribution in the Rotary Piercing Process by the Finite Element Method*, Journal of Materials Processing Technology 45 (1994) 335-340.

[54] K. Mori, K. Osakada, *Finite Element Simulation of Three-Dimensional Deformation in Shape Rolling* International Journal of Numerical Methods in Engineering 30-8 (1990) 1431-1440.

[55] K. Mori, H. Yoshimura, K. Osakada, *Simplified Three-dimensional Simulation of Rotary Piercing of Seamless Pipe by Rigid-Plastic Finite-Element Method*, Journal of Materials Processing Technology 80-81 (1998) 700-706.

[56] J. Yang, G. Li, W. T. Wu, K. Sawamiphakdi and D. Jin, *Process Modeling for Rotary Tube Piercing Application*, Materials Science & Technology 2 (2004) 137-148.

[57] K. Komori, *Simulation of Mannesmann Piercing Process by the Three-dimensional Rigid-Plastic Finite-Element Method*, International Journal of Mechanical Sciences 47 (2005) 1838-1853.

[58] Zb. Pater, W. Weronski, J. Kananecki, A. Gontrarz, *Study of the Process Stability of Cross Wedge Rolling*, Journal of Materials Processing Technology 92-93 (1999) 458-462.

[59] Q. Li, M. R. Lovell, W. Slaughter, K. Tagavi, *Investigation of the Morphology of Internal Defects in Cross Wedge Rolling* Journal of Materials Processing Technology 125-126 (2002) 248-257.

[60] Y. Dong, K. A. Tagavi, M. R. Lovell, Z. Deng, *Analysis of Stress in Cross Wedge Rolling with Application to Failure*" International Journal of Mechanical Sciences 42 (2000) 1233-1253.

[61] F. Piedrahita, L. Garcia Aranda, Y. Chastel, *Three Dimensional Numerical Simulation of Cross Wedge Rolling of Bars*, Proceedings of the 8th International Conference on Technology of Plasticity ICTP, Verona ITALY (2005).

[62] F. Pierdahita, L. Garcia Aranda, Y. Chastel, *Prediction of Internal Defects in Cross-Wedge Rolling of Bars*, Proceedings of The 9th International Conference on Material Forming ESAFORM 2006, Glasgow UK (2006) 459-462.

[63] D. A. Berazetegui, M. A. Cavaliere, L. Montelatici, E. Dvorkin, *On the Modelling of Complex 3D Bulk Metal-Forming Processes via the pseudo-Concentrations Technique. Application to the Simulation of the Mannesmann Piercing Process*, International Journal for Numerical Methods in Engineering 65-7 (2006) 1113-1144.

[64] G. Capoferri, E. Ceretti, C. Giardini, A. Attanasio, F. Brisotto, *FEM Analysis of Rotary Tube Piercing Process*, Tube & Pipe Technology (May-June 2002) 55-58.

[65] E. Ceretti, C. Giardini, A. Attanasio, F. Brisotto. G. Capoferri, *Rotary Tube Piercing Study by FEM Analysis: 3D Simulation and Experimental Results*, Tube & Pipe Technology (March-April 2004) 155-159.

[66] E. Ceretti, C. Giardini, F. Brisotto, *Development of a Simulation Model of the Tube Piercing Process and FEM Application to Improve the Quality of Seamless Tubes*, Proceedings of the 8th International Conference on Technology of Plasticity ICTP, Verona ITALY (2005).

[67] E. Ceretti, C. Giardini, A. Attanasio, *3D Simulation and Validation of Tube Piercing Process*, Proceedings of the 9th Int. Conference on Numerical Methods in Industrial Forming Processes NUMIFORM07, Porto PORTUGAL (2007).

[68] R. Pschera, J. Klarner, C. Sommitsch, *FEM Modelling of Cross Rolling Using Damage Mechanics*, Proceedings of 12th Metal Forming International Conference, Krakow POLAND (2008).

[69] XXXXXXXXX internal report, November 2005.

[70] S. Fanini, A. Ghiotti, S. Bruschi, *Evaluation of Fracture Initiation in the Mannesmann Piercing Process"* Proceedings of The 10th International

Conference on Material Forming ESAFORM2007, Zaragoza SPAIN (2007).

[71] S. Fanini, A. Ghiotti, S. Bruschi*, Prediction of the Fracture Due to Mannesmann Effect in Tube Piercing*, Proceedings of the 9th Int. Conference on Numerical Methods in Industrial Forming Processes NUMIFORM07, Porto PORTUGAL (2007).

[72] Y. Chastel, A. Diop, S. Fanini, P.O. Bouchard, K. Mocelli, *Finite Element Modelling of Tube Piercing and Creation of a Crack* International Journal of Material Forming, Springer/ESAFORM2008 (2008).

[73] Y. Chastel, A. Diop, S. Fanini, S. Bruschi, K. Mocellin, *3D Finite Element Modelling of Mannesmann Tube Piercing* Proceedings of the 9th International Conference on Technology of Plasticity ICTP, Gyeongju KOREA (2008).

[74] S. Fanini, S. Bruschi, A. Ghiotti, *Modelling of Mannesmann Fracture Initiation During Cross-Roll Piercing* Proceedings of The 12th Metal Forming International Conference, Krakow POLAND (2008).

[75] *Forge® Users' Manual*, Transvalor.